

Check for updates

Cottonseed-Derived Reusable Bio-Carbon Gel Ink for DIW Printing Soft Electronic Textiles

King Yan Chung, Di Tan, Ziyu He, Xiao Li, Jian Lu, Qingjun Yang, Xinlong Liu, and Bingang Xu*

Soft electronics textiles have garnered global attention for their wearability and promising applications in healthcare, energy devices, and artificial intelligence. Recently, direct-ink-writing (DIW) technology has shown a growing trend because of its controllability, ease of fabrication, and efficiency. However, the design novelty of printable ink for soft electronic textiles is severely hampered by the intrinsic challenges of integrating printability, conductivity, stretchability, biocompatibility, and durability. Herein, a reusable DIW bio-carbon gel ink is proposed for printing soft electronic textiles where cottonseed peptone-functionalized multi-wall carbon nanotubes (CPCNTs) exhibit high dispersibility and reactive surface groups, enabling stable cross-linking with phytic acid (PA) and polyvinyl alcohol (PVA) to form a strong ionic polymer composite. Encouragingly, the gel ink can be directly exploited to design complex circuits and versatile electronics via DIW printing on both polymeric and textile substrates. The viscoelasticity, mechanical recovery, electric properties, robustness, and stretchable architectures enable it to function as flexible circuits, smart sensors, and renewable generators. As demonstrations, multifunctional applications are presented by real-time healthcare monitoring, LED lighting, and power generation. Furthermore, this printable gel ink is effectively assembled into an integrated wearable unit for robot manipulation and real-time gesture recognition, suggesting a significant printing strategy for next-generation wearable electronics.

1. Introduction

The development of wearable electronics has increased intensively in the past decades owing to their superiority in personal

healthcare, energy devices, and robotic actuation.[1-5] The unique mechanical properties, low material cost, high flexibility, and ease of manufacturing of soft electronic textiles are widely considered as a fascinating platform for achieving next-generation wearable electronics.[6-9] However, limited electrical and mechanical properties, inferior scalable fabrication, and unsatisfactory durability still emerge due to the weakened crosslinked network and breaking of physical bonds in the polymer chains over time.[10,11] Particularly, the prevalence of green-based fabrication has survived ineffective approaches and performances because of their poor dispersibility.[12] The thick and bulky feature found in most wearables also hinders their feasibility as a subtle and comfortable integration for diverse practical applications. Recently, several studies have proposed the potential of biomaterialincorporated conductive composite^[13,14] in which protein-polymers have alternatively been a delightful option.[15-18] Notably, 3D printing techniques have shown great perspective owing to their effective and precise fabrication, but the

critical requirements of suitable ink hinder their application in soft electronic textiles^[19,20] in which the low viscosity, insufficient adhesion, and diffusion issues of latest liquid-based

B. Xu
Research Institute for Intelligent Wearable Systems
The Hong Kong Polytechnic University
Hong Kong 999077, China
E-mail: tcxubg@polyu.edu.hk
B. Xu

Research Institute for Smart Energy The Hong Kong Polytechnic University Hong Kong 999077, China

The ORCID identification number(s) for the author(s) of this article can be found under https://doi.org/10.1002/adma.202415702

© 2025 The Author(s). Advanced Materials published by Wiley-VCH GmbH. This is an open access article under the terms of the Creative Commons Attribution-NonCommercial License, which permits use, distribution and reproduction in any medium, provided the original work is properly cited and is not used for commercial purposes.

DOI: 10.1002/adma.202415702

K. Y. Chung, D. Tan, J. Lu, Q. Yang, X. Liu, B. Xu Nanotechnology Center School of Fashion and Textiles The Hong Kong Polytechnic University Hong Kong 999077, China Z. He, X. Li Department of Mathematics and Information Technology The Education University of Hong Kong Hong Kong 999077, China





development are relatively not appropriate. [21] Consequently, it is crucial to explore a suitable platform for generating direct-ink-writing (DIW) printable gel-based inks with proper viscosity, adhesiveness, and stability. This entails advancing effective conductive solvents [22] and establishing sophisticated ionic-crosslinked polymer networks. Furthermore, overcoming the intrinsic challenges of harmonizing printability, stretchability, mechanical recovery, stable electrical performance, biocompatibility, and durability remains imperative to enable DIW 3D printing technologies with versatile applications.

Recently, innovative approaches for the valorization of residual biomasses have formed the basis of the biorefinery concept, focusing on diminished wastage and recycling as integral elements of various industrial sustainability. In this regard, the rich fibrous proteins found in textile wastes (e.g., silk, wool, etc.) show promising potential as renewable resources and expand the range of biomedical applications and sustainable supply. "Cottonseed peptones" (CPs),[23] known as cottonseed protein hydrolysates, are one of the biomass coproducts obtained from proteinaceous materials in nature via biotechnological extraction, [24] consisting of numerous proteins (≈10 metric million tons), polypeptides, dipeptides, and amino acids. [25] The hierarchical structure and high hydrophilic proteins (albumins: 20.8–32.2%) of CPs offer outstanding solubility in water. [26] With such abundant nitrogen molecules, it could be expected to serve as ideal precursors to form a series of mesoporous biobased materials.^[27] Feasibly, CPs would be able to functionalize the surface of CNTs mediated with strong π – π interactions, indicating the possibility of CP as a dispersant for preparing biocompatible conductive CPCNT inks. It can be expected that the CP could possess excellent potential as a bio-friendly structural biomaterial to enhance the performance of environmentally friendly electronics at low cost and could be extensively applied in biomedical, bacteriological, sustainable supply, and bioplastic

In addition, phytic acid (PA), a naturally nontoxic organic acid derived from plants, was proposed as a biomass "gelator" to indicate improvement in both hydrogen bond interaction between polymer chains and weakened crystallization behavior by external multiple-crosslinked networks. [29,30] The naturally available crosslinked hydrogel presented versatility in obtaining functional materials with superior performance in terms of conductivity, optical transparency, and biocompatibility because of its great water-capturing and fast ion transport capability,[31] promoting high potentials for biomedicine. [32] Moreover, the six-phosphate ring structure of PA allows it to effectively be chelated to form ionic coordination interaction with metal ions and other conductive fillers to form high binding energy and strong stability. To be expected, CP-mediated CNT aqueous ink could act as the structurally enhanced conductive fillers to further strengthen the hydrogen bond interaction in water-based PA ionic hydrogel, and subsequently, enhance their conductive stability, mechanical properties, and processibility for printing wearable electronics, [33-35] together with a wide range of biological activities offered by PA, such as antibacterial, antiinflammatory, etc.[36] Conceivably, the tailorable physiochemical properties and favorable structure of this gel ink make big strides forward in the development of highly efficient Internet of Things (IoT), wearable electronics, as well as e-textiles with convenient, cost-effective, easy-production, and aesthetic features.

Herein, the work proposes an effective strategy to build biocompatible and robust biomaterial-medicated gel using CPs as a structural biomaterial and natural mediator to improve the dispersion of CNTs in aqueous solution and can naturally generate strong crosslinked water-based ionic hydrogel, which can be directly used as printable ink for DIW 3D printing soft electronics textiles. The unique feature of CP enables the highly homogeneous dispersion of CNTs in the PA-Fe/PVA polymer matrix without chemical destruction or artificial additives. Studies reveal the improvement in mechanical strength and electrical properties through strong multiple hydrogen bonding interactions, suggesting their feasibility as sensors, triboelectric nanogenerators (TENGs), and flexible circuits. The physical crosslinked structure also provides stability, recovery, and reusability with good maintenance. As demonstrated, the PA-CPCNT-Fe/PVA gel ink can be exploited as a functional device for real-time monitoring, LED lighting, and power generation. As a proof-of-concept application, versatile and integrated smart textile modules, including wearable gloves and sleeves, are facilely prepared by printing the biomaterial-carbon gel ink via DIW techniques. The etextiles with patterned sensors can be successfully used as a creative human-machine interface and artificial intelligence such as real-time gesture recognition and realizing precise control of the robotic manipulation. Therefore, this work proposed an encouraging material platform and technology of wearable soft electronic textiles, which can be widely applied to a variety of flexible multifunctional application prospects in motion monitoring, energy harvesting, wearable artificial intelligence, and humanmachine interaction.

2. Results and Discussion

2.1. Design, Synthesis, and DIW Printing of the CP-Assisted PA-CPCNT-Fe/PVA

The fabrication of the CPCNT ink and corresponding gel ink is illustrated in Figure 1a-c. Cottonseed peptone (CP) is a kind of bio-derived functional material from cotton plants. By analyzing the amino acid residue sequence of CP, ≈70% of hydrophilic residues dominate the polypeptide backbone in total.^[37] The rich hydrophilicity is expected to be intrinsically disordered by many protein disorder predictors. Additionally, CP also contains an appropriate amount of aromatic amino acid residues such as tyrosine (2.9%), tryptophan (1.2%), and phenylalanine (5.4%),[37] which are hydrophilic and may provide the capability to obtain a strong π – π interaction with CNTs (Figure 1a). The coexistence of hydrophilic and hydrophobic groups makes it amphipathic and endows it with the ability to reduce the surface energy of CNTs. Inspired by these unique features, it was reasoned that CP could act as a dispersant and stabilizer for constructing a biocompatible aqueous ink with high colloidal stability. As expected, a homogeneous CNT dispersion was yielded by ultrasonicating the CP solution and CNTs. To achieve high flexibility, the stable CPCNT electroconductive ink could be used as the aqueous solvent for fabricating water-based hydrogel. Briefly, it was added to the preprepared glycerol-ionic solution containing phytic acid (PA) and metal salts (FeCl₃) under continuous stirring. Poly(vinyl alcohol)

1521495, 0, Downloaded from https://advanced.onlinelibrary.wiley.com/doi/10.1002/adma.202415702 by HONG KONG POLYTECHNIC UNIVERSITY HU NG HOM, Wiley Online Library on [26/09/2025]. See the Terms and Conditions (https://onlinelibrary.wiley.com/doi/10.1002/adma.202415702 by HONG KONG POLYTECHNIC UNIVERSITY HU NG HOM, Wiley Online Library on [26/09/2025]. See the Terms and Conditions (https://onlinelibrary.wiley.com/doi/10.1002/adma.202415702 by HONG KONG POLYTECHNIC UNIVERSITY HU NG HOM, Wiley Online Library on [26/09/2025]. See the Terms and Conditions (https://onlinelibrary.wiley.com/doi/10.1002/adma.202415702 by HONG KONG POLYTECHNIC UNIVERSITY HU NG HOM, Wiley Online Library on [26/09/2025]. See the Terms and Conditions (https://onlinelibrary.wiley.com/doi/10.1002/adma.202415702 by HONG KONG POLYTECHNIC UNIVERSITY HU NG HOM, Wiley Online Library on [26/09/2025]. See the Terms and Conditions (https://onlinelibrary.wiley.com/doi/10.1002/adma.202415702 by HONG KONG POLYTECHNIC UNIVERSITY HU NG HOM, Wiley Online Library on [26/09/2025]. See the Terms and Conditions (https://onlinelibrary.wiley.com/doi/10.1002/adma.202415702 by HONG KONG POLYTECHNIC UNIVERSITY HU NG HOM, Wiley Online Library on [26/09/2025]. See the Terms and Conditions (https://onlinelibrary.wiley.com/doi/10.1002/adma.202415702 by HONG KONG POLYTECHNIC UNIVERSITY HU NG HOM Wiley Online Library on [26/09/2025]. See the Terms and Conditions (https://onlinelibrary.wiley.com/doi/10.1002/adma.202415702 by HONG KONG POLYTECHNIC UNIVERSITY HU NG HOM Wiley Online Library on [26/09/2025]. See the Terms and Conditions (https://onlinelibrary.wiley.com/doi/10.1002/adma.202415702 by HONG KONG POLYTECHNIC UNIVERSITY HU NG HOM Wiley Online Library on [26/09/2025]. See the Terms and Conditions (https://onlinelibrary.wiley.com/doi/10.1002/adma.202415702 by HONG FOLYTECHNIC UNIVERSITY HU NG HOM Wiley Online Library on [26/09/2025]. See the Terms and Conditions (https://onlinelibrary.wiley.com/doi/10.1002/adma.202415702 by Hong Folyt Hu Hong Folyt Hu Hong Folyt Hu

and-conditions) on Wiley Online Library for rules of use; OA articles are governed by the applicable Creative Commons License

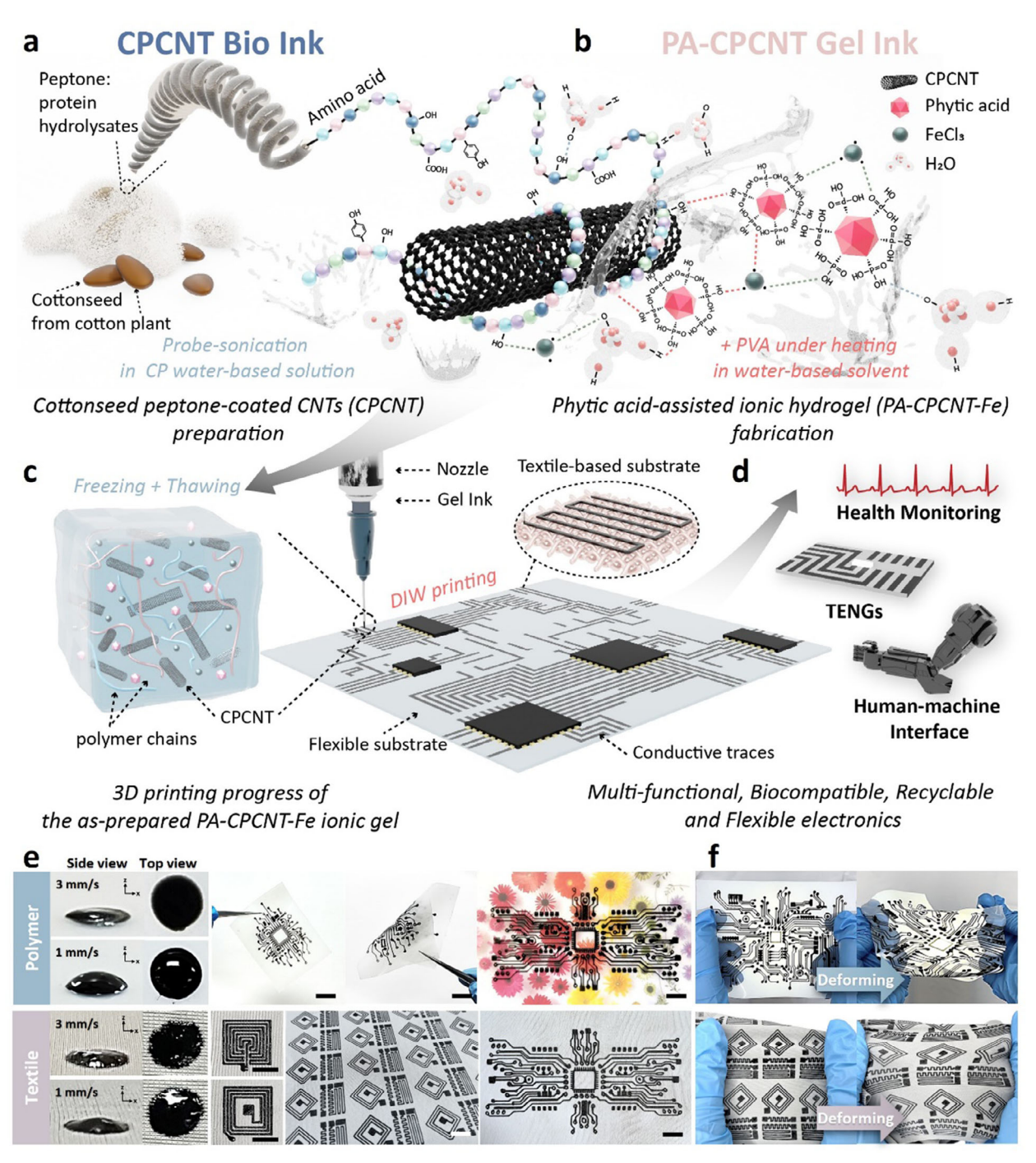


Figure 1. Schematic illustration of a) the residue sequence of the cottonseed peptone driven from cottonseed and its mediation to the surface of CNT in forming CPCNT gel-ink; b) the fabrication of PA-CPCNT-Fe/PVA gel ink with the addition of PA, FeCl_{3,} and PVA. c) DIW schematic printing of the PA-CPCNT-Fe/PVA gel ink on different flexible substrates. d) Peptone-derived carbon-gel ink for flexible circuits and multiple applications. e) Top and side images of the PA-CPCNT-Fe/PVA gel ink on polymer and textile substrate via DIW printing at different printing speeds and various printing demonstrations. f) Stretchability of the PA-CPCNT-Fe/PVA printed flexible electronics (Top: polymer; Bottom: textile substrate).

(PVA) was then added to initiate polymer cross-linking and interaction under heating. The ionic hydrogel could be cured by freezing and thawing, in which the hydroxyl groups on PVA chains reacted with the CPCNT, PA, and FeCl₃, resulting in a continuous and stable structure (Figure 1b). The detailed procedure of

preparations can be found in the experimental section. Taking the good viscosity of hydrogel, the fabricated PA-CPCNT-Fe/PVA gel ink could be used as printable ink for flexible circuits and electronics. As illustrated in Figure 1c, a demonstration of direct ink writing (DIW) is successfully presented on both polymeric and





textile substrates. Owing to its flexibility, conductivity, stability, and turnability, the PA-CPCNT-Fe/PVA gel ink could be feasible in the fields of health tracking, energy harvesting, conductive circuits, and human-machine interaction (Figure 1d). Importantly, the printability of the PA-CPCNT-Fe/PVA bio-mediated gel ink on various substrates such as polymeric and textile materials is confirmed in Figure 1e,f. The swelling behavior and thickness of gel on different substrates were controlled by the printing speed in which a higher diameter could be found in the cross-section at a lower speed (Figure 1e, left). Significant printing quality was received both for simple and complicated circuit patterns. The SEM images of the printed textile ensured its printing quality and that the gel could be successfully coated on the textile surface with penetration (Figure S1, Supporting Information). A demonstration of DIW writing on textiles using carbon gel is also shown in Video S1 (Supporting Information). Furthermore, printed flexible electronics showed good adhesiveness and flexibility upon deformation (Figure 1f), indicating the remarkable feasibility of PA-CPCNT-Fe/PVA gel ink in the development of future flexible electronics and e-textiles.

2.2. Morphology, Characterization, and Printability of PA-CPCNT-Fe/PVA

Taking advantage of the softness, flexibility, and adhesiveness of hydrogels,[38-41] a biomass-based hydrogel preparation using PVA and PA was adopted in this study because of its excellent mechanical stability, processability, biodegradability, and high environmental safety.[30,32,33,42] The carbon-gel ink was prepared by a one-step sol-gel synthesis of CPCNT and PA-Fe/PVA. Briefly, the pre-prepared CPCNT aqueous ink was added to the ionic polymer matrix under continuous stirring, and cross-linking was initiated under heat which chemical structure is addressed in Figure S2 (Supporting Information). Subsequently, the PA-CPCNT-Fe/PVA mixture was cured to obtain the hydrogels via freezing (Figure 2a). As schematically illustrated in Figure 2b, the interaction mechanism between CPCNTs ink and polymer chains is constructed by the addition of PA which acts as a mediator to provide favorable conditions for enzyme or protein immobilization.[43] Concerning PA-Fe/PVA hydrogel, a promising crosslinking could be found upon bonding anions of PA to cations of such a polymer, and through the formation of intermolecular hydrogen bonds. This was attributed to the presence of hydroxyl-bearing phosphoric groups in the PA compound.[32] When PVA and PA were introduced to the CPCNT aqueous ink, the high functional groups, including amide, carboxyl, and hydroxyl on CPCNTs, hydroxyl on PA, and hydroxyl on PVA, interacted intensively with each other to form a complex through dense arrays of covalent and non-covalent bonds. The hydrogen bonds in CPCNT and PVA segments were further reconstructed and strengthened by the rich hydroxyl groups on PA with additional physical cross-linking^[44] and the crystallization degree was reduced simultaneously,^[45] owing to the strong gelatinization of PA molecules enlarging the space between PVA chains (Figure S3, Supporting Information). Besides, the large number of phosphoric acid groups in PA was capable of reacting with cations to form ionic bonds, generating a continuous conductive network scaffold between CPCNT and hydrogel chains.[46]

Meanwhile, PA molecules strongly interacted with ferric (Fe³⁺) ions by ionic coordination to further improve the crosslinking degree of the hydrogel.^[30] As a result, the obtained PA-CPCNT-Fe/PVA gel maintained stable conductivity, adhesiveness, mechanical strength and self-recovery, which will be discussed further in the next section.

To verify the appearance of hydrogel, SEM images were taken with different resolutions showing the CPCNTs and the porous structure. It can be observed that many CPCNTs were dispersed and hidden in the pores of the obtained hydrogel (Figure 2c), suggesting the dispersion in the gel and interaction with the polymer chains. A dense dispersion of CPCNT was seen and hidden on the surface (Figure 2c,i,ii) while pores were seen in the inner of the hydrogel (Figure 2c,iii,iv), offering satisfactory softness and flexibility to the gel ink. The breathability of hydrogel is also examined by printing on fabric (Figure S4, Supporting Information). The homogeneous dispersion of CNTs in the hydrogel composite was attributed to the assistance of CP in regulating interfacial interactions, overcoming the massive van der Waals forces and strong π - π interactions between CNTs. Figure 2d (left) shows a CPCNT gel-ink with welldispersion. Moreover, it could maintain good dispersion without quick precipitation by simple handshaking; whilst drops of the as-prepared CPCNT gel-ink could rapidly spread in water quickly, promoting the benefits of cottonseed peptone in modifying CNTs and its good dispersity in water (Video S2, Supporting Information). The resultant mixture showed intensive stability for 1 week without evident precipitation (Figure \$5, Supporting Information).

To further investigate the interaction characterization of the CPCNTs, transmission electron microscopy (TEM) was employed to directly observe the adsorption of CP on the CNT surface (Figure 2d, right). From the TEM image with higher resolution, an inner crystalline part and an outer amorphous part could be distinguished, which can be ascribed to the walls of the CNT and the adsorbed CP, respectively. To reveal the advancement of CP in CNT dispersion, UV-vis spectroscopy was performed where a characteristic peak of protein was shifted from 267 nm in CP to 256 nm in the CPCNT dispersion spectrum with a broader shape, indicating the interaction between the aromatic groups and the surface of CNTs (Figure S6a, Supporting Information). Notably, CP had the highest absorbance peak and was comparable to other bio-surfactants, such as sericin and other food or plant types of peptones, attributing the unique feature of CP (Figure S6b, Supporting Information). This affirmed the superior capability of CP to disperse CNTs with a high degree of freedom in the water, owing to the intrinsically disordered protein structure.

Correspondingly, the possibility of physical structure and the formation of hydrogen bond crosslinking networks in the CPCNT and PA-CPCNT-Fe/PVA can be verified by the FTIR spectrum in Figure 2e,f. The amide I peak of CPCNT slightly shifted from 1654 to 1677 cm⁻¹ as compared to pristine cotton-seed peptone, promoting the hydrogen bond interaction between the CP and CNT surface. The peaks at 3286 cm⁻¹ were ascribed to the stretching vibration of —OH groups in the CPCNT/PVA, confirming the formation of polymer chains and hydrogen bonds between the CPCNT surface and PVA. Then, after the addition of PA and Fe³⁺ ions, the wavenumber movement for

15214095, 0, Downloaded from https:

anced.onlinelibrary.wiley.com/doi/10.1002/adma.202415702 by HONG KONG POLYTECHNIC UNIVERSITY HU NG HOM, Wiley Online Library on [26/09/2025]. See the Terms and Conditions (https://onlinelibrary.

and-conditions) on Wiley Online Library for rules of use; OA articles are governed by the applicable Creative

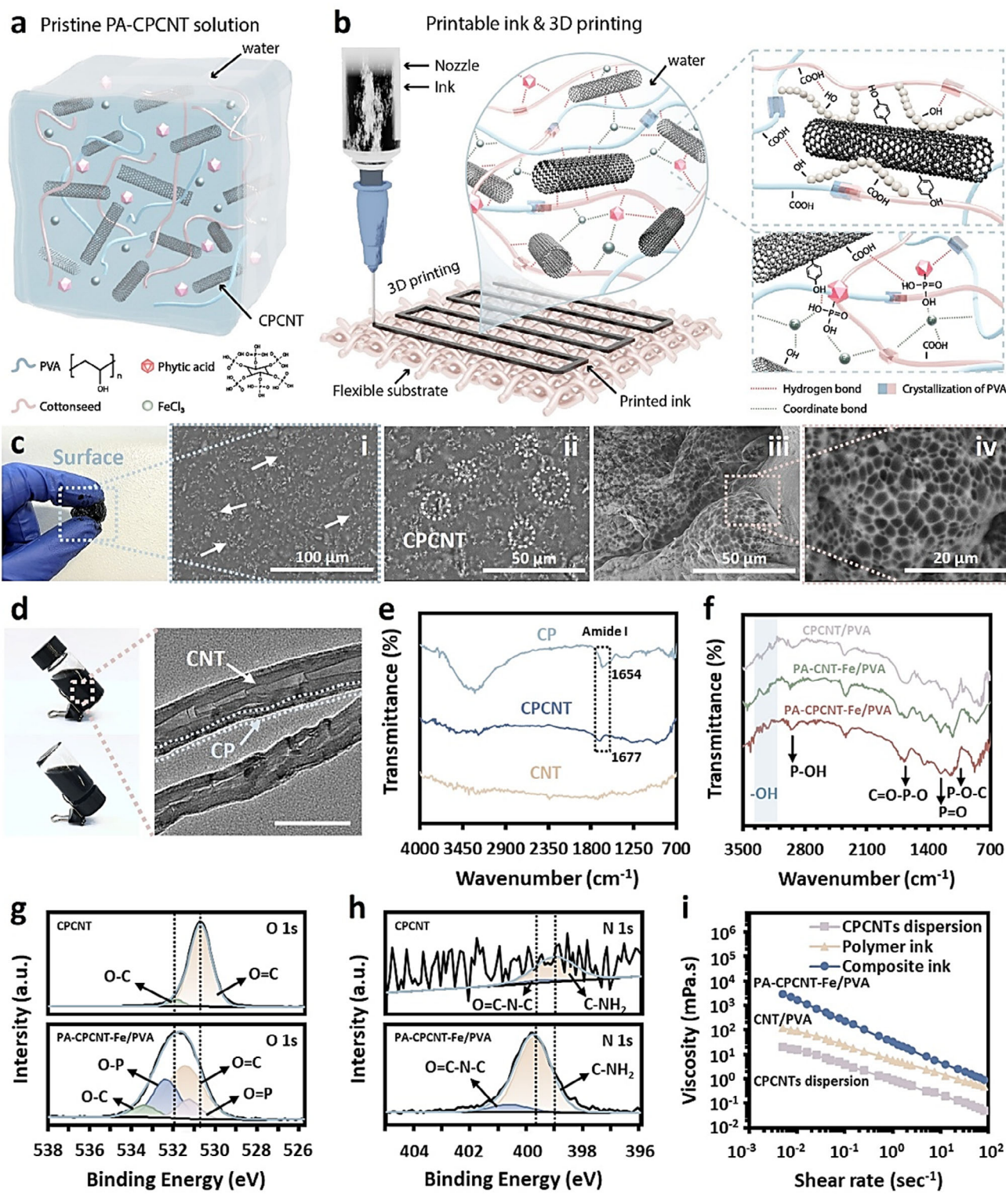


Figure 2. Characterization of the CPCNTs and PA-CPCNT-Fe/PVA gel ink. Schematic illustrations of a) the polymerization and b) the printing process and interactive bonding of the PA-CPCNT-Fe/PVA hydrogel. c) Photographs of the PA-CPCNT-Fe/PVA hydrogel and SEM image of PA-CPCNT-Fe/PVA hydrogel: i, ii) surface and iii, iv) inner-section at different resolutions. d) Typical photographs of CPCNTs suspension with 5 mg mL⁻¹ (left) and TEM image of uniformly dispersed CNTs prepared from the CPCNT ink showing a CNT coated with CP shell (right). FTIR spectra of e) pristine CP, CPCNT, and pristine CNT, and f) CPCNT, PA-CNT-Fe/PVA and PA-CPCNT-Fe/PVA. XPS spectra of g) O 1s and h) N 1s for CPCNT and PA-CPCNT-Fe/PVA. i) Viscosity—shear stress of the CPCNTs dispersion, CNT/PVA, and PA-CPCNT-Fe/PVA gel.



the adsorption peak of -OH group was shifted to 3210 cm⁻¹ in PA-CPCNT-Fe/PVA. A characteristic peak at 1642 cm⁻¹, 1259 cm⁻¹, and 1083 cm⁻¹ appeared in PA-CPCNT-Fe/PVA, corresponding to the stretching vibration of C=O-P-O, P=O, P-O-C originating from PA molecules.[30,47] Besides, the stretching vibration of -OH groups was shifted from 3259 to 3210 cm⁻¹ by the addition of Fe³⁺ ions which was attributed to the formation of ionic coordination interactions between the —OH groups on the PVA polymer chains and the Fe³⁺ ions from FeCl₃ [48] whilst the stretching vibration of C=O-P-O, P=O, P-O-C shifted toward to a large offset and weak adsorption which was attributed to the formation of ionic coordination and increased formation of hydrogen bonds between PA molecules, Fe³⁺ ions, CPCNT and PVA polymer chains. Additionally, Raman spectrum confirmed the MWCNTs in the CPCNT ink where typical peaks of D band, G band, and 2D were determined, respectively. As shown in Figure \$7 (Supporting Information), a peak of 2925 cm⁻¹ refers to the stretching mode of C–H bonds and O-H bonds of stretching vibration area are within the range of 3050-3600 cm⁻¹.[49] Regarding the comparison of the PA-CNT-Fe/PVA and PA-CPCNT-Fe/PVA, the characteristic D peak and G peak were shifted from 1338 to 1348 cm⁻¹ and 1577 to 1582 cm⁻¹, respectively. It reveals that more defective structures on CPCNT make it easier to form a strong interface interaction with PA-Fe/PVA, thereby obtaining a stronger mechanical enhancement effect on the composites, which will be discussed

High-resolution XPS spectroscopy was employed to further analyze the chemical states of elements and the interaction mechanism of the CPCNT and the hydrogel matrix. As seen in Figure 2g,h, the O 1s spectrum of CPCNT and PA-CPCNT-Fe/PVA is given in which the O 1s spectra of CPCNT are deconvoluted to two characteristic peaks of O=C (530.95 eV) and O-C (532.08 eV), while the N 1s spectra include two characteristics peaks of C-NH2 (399.09 eV) and O=C-N-C (399.74 eV). After adding CPCNTs dispersion in the PA-Fe/PVA, the peaks of O=C, O-C, C-NH, and O=C-N-C of the obtained hydrogel shifted to higher binding energy (from 530.95 to 531.56 eV, 532.08 to 533.52 eV, 399.09 to 399.85 eV, and 399.74 to 400.76 eV, respectively), compared with CPCNT, suggesting the strong interaction between the hydroxyl group of PA-Fe/PVA and the hydroxyl group, amino group, and carboxyl group of CPCNT.^[50,51] The C 1s addressed in Figure S8a (Supporting Information) also confirm the above interaction in which the sp2 bonding suggests the carbon atoms and both C—O and C=O bonding appear in PA-CPCNT-Fe/PVA. Besides, the presence of O-P bonding (532.48 eV) and O=P bonding (531.39 eV) also suggested the obtained hydrogel is rich in phosphate groups on their surface (Figure S8b, Supporting Information), as well as the binding energy of P 2p band (P—O bonding: 133.90 eV).[50,52]

Consequently, the printability of the inks was then analyzed by studying the shear-thinning behavior of rheology. The distinct shear-thinning behavior can be seen in all the inks, as shown in Figure 2i, which is necessary for smooth extrusion during DIW. In addition, the PA-CPCNT-Fe/PVA ink showed the highest apparent viscosity than pure CNT/PVA ink at the same composite concentration. This enhancement is likely to be owing to the strong hydrogen bonding and physical interactions

(e.g., entanglement) among the CPCNT and other components with high aspect ratios, as shown in the Figure S9 (Supporting Information).^[30,34]

2.3. The Conductivity, Adhesiveness, Mechanical Properties, and Repeatable Performance of PA-CPCNT-Fe/PVA

Beneficial from the above-discussed functional bonding and interaction in the PA-CPCNT-Fe/PVA hydrogel, the conductive performance of the carbon gel-ink was shown by lighting up LEDs with a printed circuit (Figure 3a). Specifically, the obtained gel ink showed a relatively low percolation threshold, and the electrical conductivity followed the addition of CPCNT content (Figure 3b). Nearly threefold improvement in conductivity can be found from 2.5 S m⁻¹ of pure PA/PVA to 8 S m⁻¹ of PA-CPCNT-Fe/PVA (Figure 3c). The positive effect of the electrical conductivity can be explained by the homogenous dispersion of CPCNT with a high aspect ratio and the formation of a continuous filler network with gradually decreased spacing between CNT and PA-Fe/PVA. A dramatic improvement is found in CP regulation in Figure \$10 (Supporting Information). Increasing the loadings can create additional hopping sites for electron transfer. An increasing trend in electric conductivity was found with increasing the CPCNTs from 0.1 to 0.5 wt.% and reaching a maximum level at the 1 wt.% of CPCNTs in the hydrogel.

Encouraged by the hydrogen bonding and interactions, the adhesiveness of the hydrogel was also studied for its bonding strength on the textile-based substrate. Adhesion is a supramolecular phenomenon that includes a combination of topologies of connection, chemistries of bonds, and mechanics of dissipation.^[53] It was taken by gelating an adherent layer between solid surfaces (e.g., a pair of glass plates) with a contact area of 2 cm², and then, weight was applied for measurement. The results supported the adhesive ability to sustain and lift a load of 1 kg in out-of-plane and in-plane directions, respectively (Figure 3d, right). Subsequently, the adhesive principle is illustrated in Figure 3d (left) with SEM image which includes 1) the mechanical interlock generated by the roughness of solid adhesive layers, where PA-CPCNT-Fe/PVA gel fills the pits and then cures into a rigid adhesive layer, 2) densely packed stable interaction formed between the -OH groups of PA-CPCNT-Fe/PVA and substrate, and 3) strong energy dissipation that contains the separation of intertwined ionic polymer chains, slipping and detaching of the polymers from the surface of CPCNT fillers.

Notably, stress could be efficiently dissipated between CPCNT and PA-Fe/PVA polymer via their firm interfacial interactions under deformation, giving rise to a hydrogel with toughness and flexibility. The mechanical properties of PA-CPCNT-Fe/PVA with different CPCNT ratios were investigated correspondingly via a tensile test (Figure 3e). As expected, a remarkable improvement in tensile strength and elongation could be found by the incorporation of CP, PA inclusions, and Fe³⁺. The maximum stress of pristine PVA hydrogel without fillers was 197.35 kPa at 359% strain, while those of composite hydrogel PA-PVA, CNT/PVA, PA-CNT-Fe/PVA, and PA-CPCNT-Fe/PVA were 780.19 kPa at 387% strain, 247.35 kPa at 424% strain, 330.23 kPa at 564% and 1152.5 kPa at 933% strain, respectively. An obvious improvement

1521495, 0, Downloaded from https://advanced.onlinelibrary.viety.com/doi/10.002/adma.20241579.02 by HONG KONG POLYTECHNIC UNIVERSITY HU NG HOM, Wiley Online Library on [26/09/2025]. See the Terms and Conditions on Wiley Online Library viety.com/emer-and-conditions) on Wiley Online Library on [26/09/2025]. See the Terms and Conditions on Wiley Online Library viety.com/emer-and-conditions) on Wiley Online Library viety.com/emer-and-conditions) on Wiley Online Library viety.com/emer-and-conditions on Wiley Online Library viety.c

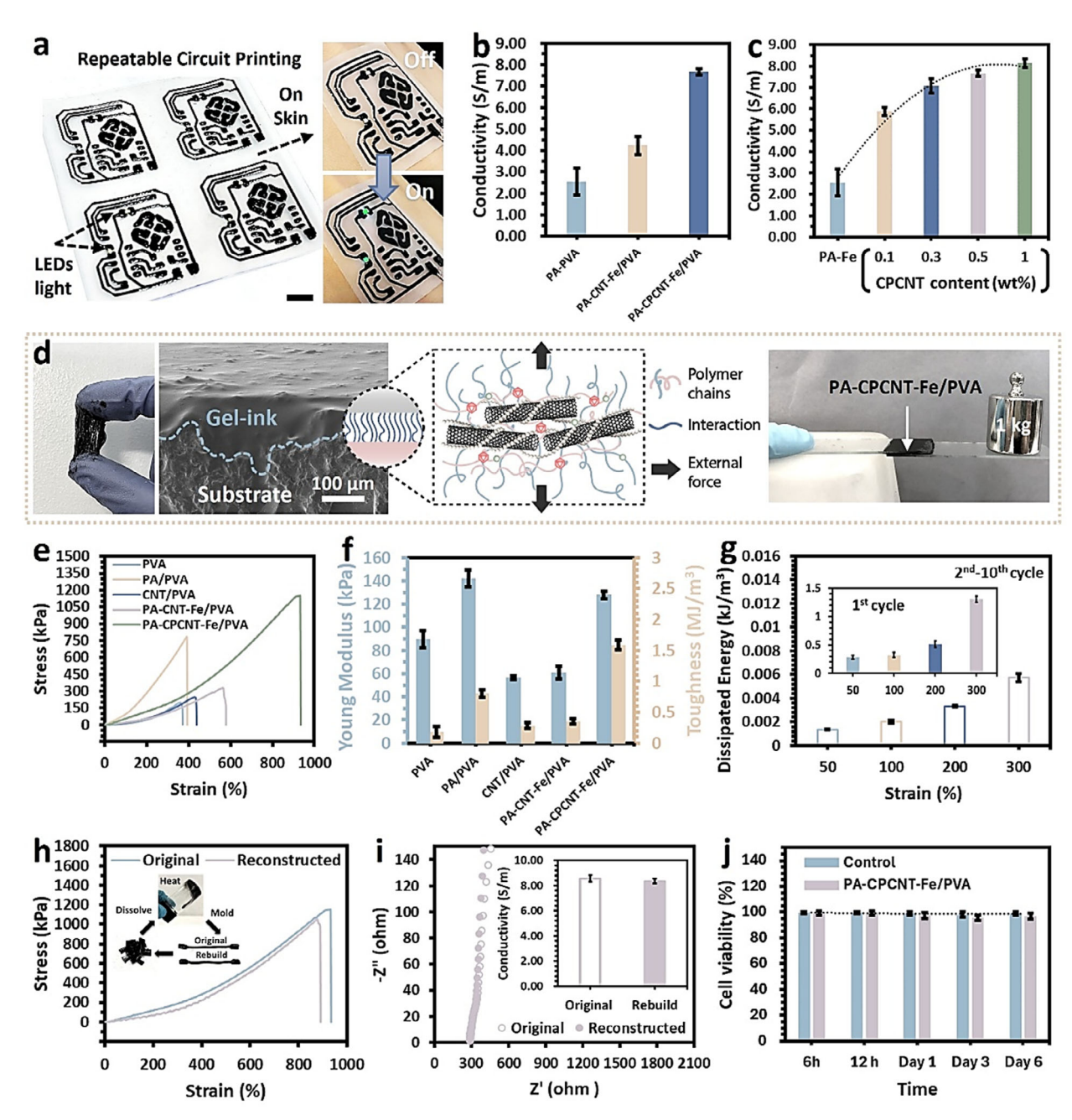


Figure 3. Hydrogel performance of the PA-CPCNT-Fe/PVA gel ink. a) The electric performance of the PA-CPCNT-Fe/PVA gel as a conductive circuit via DIW printing. Conductivity of b) hydrogel with different additions and c) PA-CPCNT-Fe/PVA with varying CPCNTs content. d) Photograph and SEM image of PA-CPCNT-Fe/PVA hydrogel showing the adhesiveness between the gel-ink and the surface of the solid layer and ability against 1 kg of loading. e) The tensile stress—strain curves of PVA, PA/PVA, CNT/PVA, PA-CNT-Fe/PVA, and PA-CPCNT-Fe/PVA hydrogels. f) Comparison of Young's modulus, and toughness of the PVA, PA/PVA, CNT/PVA, PA-CNT-Fe/PVA, and PA-CPCNT-Fe/PVA hydrogels. g) Energy dissipation of PA-CPCNT-Fe/PVA after the cyclic stretch. h) Tensile stress—strain curves of PA-CPCNT-Fe/PVA before and after reconstruction. Inset: the reconstruction process. i) Electrical conductivity of PA-CPCNT-Fe/PVA before and after reconstructing. j) Cell viability (%) of the PA-CPCNT-Fe/PVA in 6 h, 12 h, 1 day, 3 days and 6 days, respectively.

in toughness could be seen between PA-CPCNT-Fe/PVA and other samples (Figure 3f). These results indicated that the introduction of CP assisted in the improvement of the mechanical performances of PVA-based hydrogel. The variation in mechanical

strength is also investigated under different CPCNT contents in Figure S11a (Supporting Information) in which higher stress can be received by increasing the CPCNT loadings from 0.1 to 1 wt.% because of more compact fillers and bonding networks; whilst





3 wt.% of CPCNT decreases the mechanical strength because of the agglomeration. The results of the CPCNT hydrogels containing PA and/or Fe3+ ions were quantitatively assessed to investigate the effects of PA and Fe³⁺ contents on the mechanical properties. As presented in Figure S11b (Supporting Information), with the increase in the addition of Fe³⁺ content to 0.5 wt.%, the tensile strength of PA-CPCNT-Fe/PVA hydrogels gradually increased, while a decreasing trend was found on the contrary with a further increase of the Fe3+ content to 1 wt.%. In addition, the stress-strain curve of CPCNT hydrogel with PA content from 0 to 35 wt.% showed an increasing strength while a slight decrease was found with PA content > 30 wt.% (Figure S11c, Supporting Information). Both phenomena confirmed the appropriate addition of Fe³⁺ and PA contents could, in turn, improve the tensile properties of hydrogels in which the former could assist in the amount increase of dynamic crosslinking interaction by forming the ionic coordination between PA and Fe³⁺, and the latter could effectively increase the amount of cross-linking sites to form hydrogen bonds between PA and PVA, and ionic coordination between PA and Fe³⁺, generating a denser crosslinked network. Besides, it is worth noting that the tensile strength of waterbased hydrogel was strengthened with the increase of freezethawing cycle numbers (Figure S11d, Supporting Information).

Flexible wearable devices should require outstanding robustness properties for the development of next-generation electronics. The mechanical deformability and recovery performance of the PA-CPCNT-Fe/PVA were discussed based on the designed physical and chemical crosslinks. The PA-CPCNT-Fe/PVA gel ink exhibited excellent deformability and low hysteresis owing to the synergistic effect of different interactions produced by the components. The energy dissipation was evaluated by the cyclic loading-unloading test at different strains, which was contributed by the internal friction during the movement of polymer chains as well as the breaking of hydrogen bonds and coordination bonds. Figure \$12 (Supporting Information) shows its 1st tensile loading-unloading cycle at different strain levels with a linear increase in stress. Although slight energy dissipation was observed in the 1st loading-unloading cycle at different strains (Figure 3g, inset), no visible dissipated energy was found in the following successive tensile cycles with a very low value of <0.01 kJ m⁻³ (Figure 3g), indicating substantial cross-linking points inside the hydrogel and excellent strainstress recovery.^[54] The corresponding stress and dissipated energy of each loading-unloading cycle from 2nd to 10th at 100% and 400% strain are addressed and compared in Figure S13a-d (Supporting Information), respectively. The maximum stress decreased slowly and remained constant while the dissipated energy was kept in a superior low range, suggesting the reversible interchain interactions. [53,55] Interestingly, equivalent dissipated energy was found in the second or even more 10 successive loading-unloading cycles after storage at room temperature in which a higher interval time led to a better recovery (Figures S14 and S15, Supporting Information). It is ascribed to the fact that the hydrogen bond and ionic coordination interactions in the hydrogel network structure temporarily dissociated as reversible "sacrificial" bonds, suggesting the favorable performances of mechanical strength, toughness, fatigue resistance, and self-recovery in practical applications. In general, the above results indicated that the prepared Fe_{0.5}-PA₂₅-CPCNT₁-PVA hydrogels have favorable conductive, mechanical, and resilience performance.

Additionally, being a water-based hydrogel, it allows for reconstruction through a physically crosslinked process, aligning with the advancement of reusable eco-friendly electronics. The reconstruction process was started by cutting the fabricated hydrogel into millimeter-sized pieces which were fragmented by an external force at 50 °C. The dried hydrogel pieces were placed into the glass bottle with DI water. Under heating, the hydrogel pieces transformed into a gel state and could be cured again after the freeze-thawing process (Figure 3h, inset and S16). Significantly, the reconstructed PA-CPCNT-Fe/PVA gel maintained consistent performance to the original gel in which comparable mechanical properties and invisible decrease could be seen in the electric conductivity (Figure 3h,i). Therefore, this gel-ink could be potentially reused in the printing process (Figure S16, Supporting Information). Besides, biocompatibility is a prerequisite property for wearable or attachable electronics which was analyzed by cell viability test. No visible damage could be cultured in the high-resolution images of the living cells with or without PA-CPCNT-Fe/PVA sample (Figure \$17, Supporting Information). Generally, cell viability of more than 80% is regarded as good biocompatibility. [56] Thus, the maintenance of cell viability in PA-CPCNT-Fe/PVA samples was kept after 6 h, 12 h, 1, 3, and 6 days (Figure 3j), indicating a harmless capability.

2.4. Sensing Performances of the PA-CPCNT-Fe/PVA as E-Textiles

As displayed in Figure 4a, the relative resistance changes of the PA-CPCNT-Fe/PVA printed textile sensor result in a high linearity of $R^2 = 0.9923$ and $R^2 = 0.9994$ from the strain of 0% to 300% and 300% to 500%, respectively. The linear sensitive ranges were attributed to the homogeneously distributed conductive fillers and highly ordered chain network in the composite. The enhancement in resistance change was shown through comparisons with other test samples (Figure S18a, Supporting Information). Moreover, an increased relative resistance change was observed with higher addition of CPCNT (Figure \$18b, Supporting Information). The response mechanism of the PA-CPCNT-Fe/PVA can be mainly summarized as the structure transformation of the conductive network constructed by CPCNTs, which is explored in Figure 4b. Within a narrow strain range at the early stage, relative displacement occurs among the fillers, but free electrons pass through the breakpoints of the conductive network according to the tunneling effect, leading to a small resistance change. The entire conductive network can be disintegrated by the continuous expansion of the filler spacings. Upon stretching, the interconnected conductive fillers started to be separated from each other and even reached a blocking of electron transmission when the expansion along the stretching direction was further dominated, resulting in a continuous and sharper rise of the resistance.

Figure 4c captures the strain-sensing performance and repeatability of the e-textile under different levels of continuous stretching where a broad strain-sensing range is noticed from 100% to 450%. When tensile stress was applied to the PA-CPCNT-Fe/PVA hydrogel, the overlap among adjacent CNTs was decreased, resulting in an increment in relative resistance.

1521495, 0, Downloaded from https://advanced.onlinelibrary.viety.com/doi/10.002/adma.20241579.02 by HONG KONG POLYTECHNIC UNIVERSITY HU NG HOM, Wiley Online Library on [26/09/2025]. See the Terms and Conditions on Wiley Online Library viety.com/emer-and-conditions) on Wiley Online Library on [26/09/2025]. See the Terms and Conditions on Wiley Online Library viety.com/emer-and-conditions) on Wiley Online Library viety.com/emer-and-conditions) on Wiley Online Library viety.com/emer-and-conditions on Wiley Online Library viety.c

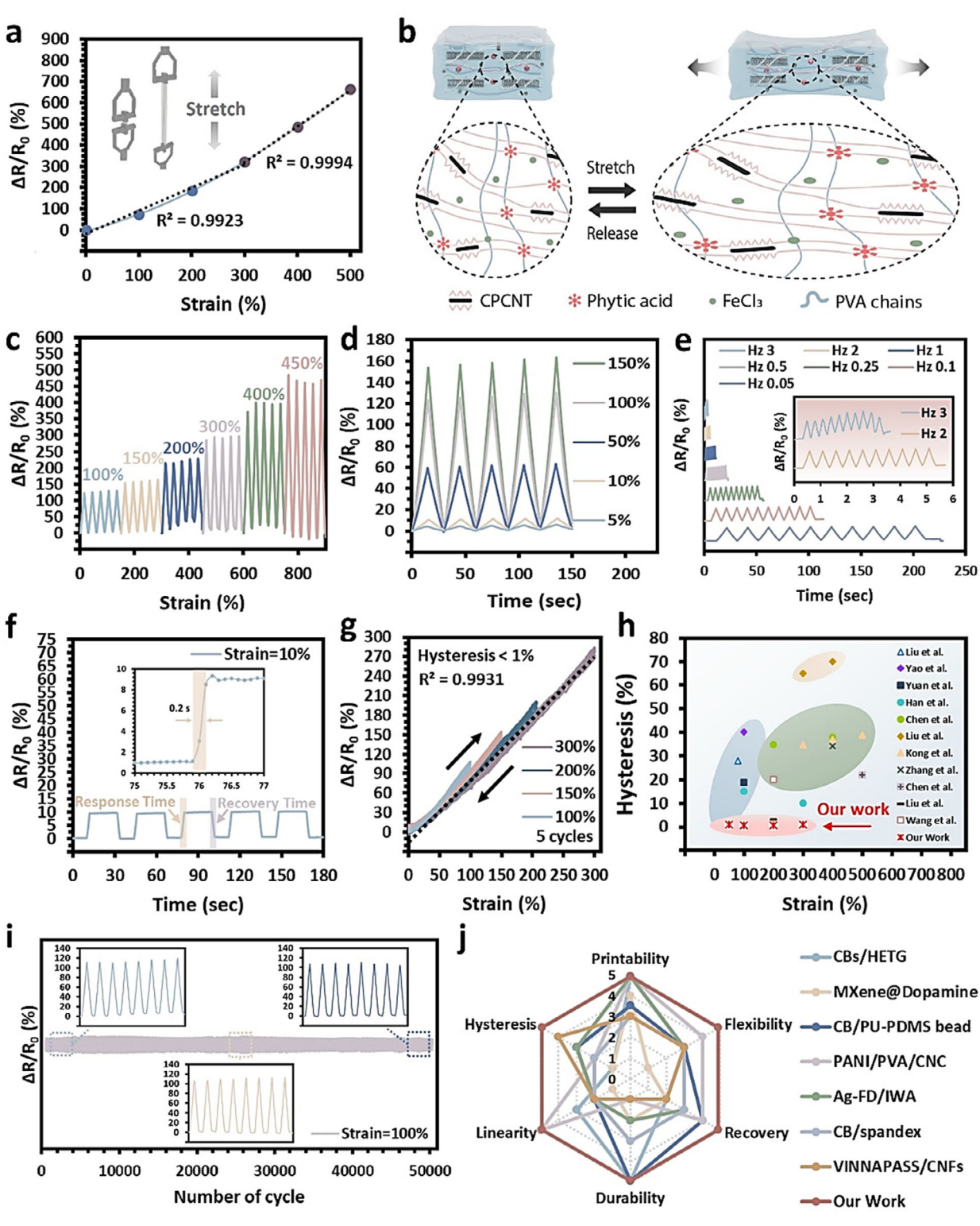


Figure 4. Working mechanism and sensing performance of the PA-CPCNT-Fe/PVA e-textile. a) Typical relative resistance versus strain curve of PA-CPCNT-Fe/PVA. b) Schematic illustration of the sensing mechanism. Time-dependent relative resistance variations of PA-CPCNT-Fe/PVA under various cyclic strains at c) high stretch ranges and d) low stretch ranges. e) Relative resistance changes of the PA-CPCNT-Fe/PVA at different frequencies. f) Response curve of the PA-CPCNT-Fe/PVA with an applied strain of 10% shows a response time of 200 ms. g) Load-unloading hysteresis curve of the PA-CPCNT-Fe/PVA under five cyclic cycles at different strains. h) Comparison of the hysteresis and strain between the PA-CPCNT-Fe/PVA e-textile with other previous works. i) Durability of the relative resistance change of the PA-CPCNT-Fe/PVA printed e-textile in 50000 stretching/relaxation cycles at 100% strain. j) Comparison between our work and recently reported gel-ink-based fabric sensing devices considering printability, flexibility, recovery, durability, linearity, and hysteresis.





Once the stress was withdrawn, the polymer network and PA-CPCNT-Fe cross-linkages rapidly contracted to their initial state, restoring the relative resistance of PA-CPCNT-Fe/PVA hydrogel to its initial resistance. The sensor underwent 5 stretchrelease cycles at small-level strains (5%, 10%, 50%, 100%, and 150%, respectively), and the corresponding reliable resistive responses are listed in Figure 4d. The electrical response at different frequencies (0.05, 0.1, 0.25, 0.5, 1, 2, and 3 Hz, respectively) was also addressed, suggesting the availability of the sensor for various strain-induced application scenarios (Figure 4e). A response time of <200 ms and a recovery time of 62 ms was defined at 10% strain of the sensor under a stretching speed of 17 mm s⁻¹ (Figure 4f). The response time is less than 400 ms, which matches the reaction time of human skin.^[57] In addition, from the low energy dissipation discussed before, the stretchrecovery properties of the PA-CPCNT-Fe/PVA are investigated in Figure 4g. It belonged to the high-density hydrogen bonds and the synergistic effect of different interactions between the components in the hydrogel. As shown in Figure 4h, it is encouragingly noted that our PA-CPCNT-Fe/PVA exhibits a remarkably low hysteresis under a wide range of strains (100% to 300%), which is superior to the reported hydrogel developments, [58-68] showing excellent matching between the internal friction and the change of stress. An irreversible relative displacement footprint was normally generated in higher mechanical change due to the unrecovered chains in the polymer matrix which further ensured the advancement of stability in this carbon gel. Besides, the device exhibited high repeatability and reliable stability through ≈50000 stretching-relaxation cycles at 100% (Figure 4i). Generally, the entire conductive network returns to its original state when the applied strains are released, although a few hydrogen bonds can be irreversibly destroyed via polymer chain slippage during the deformation. Furthermore, the significant characteristics of this sensor were investigated by comparing with recently reported gel-ink-based fabric sensing devices.^[69–75] As a consequence, a radar chart of comprehensive performance comparison including printability, flexibility, recovery, durability, linearity, and hysteresis, is presented in Figure 4j. Each property was divided into 1-5 grades, and the judging standards for the grading and detailed information of each work are shown in Tables S1 and S2 (Supporting Information), respectively. By comparing these gel-ink-based fabric sensing devices, our work exhibited the highest performance in all indexes as compared to the reported works, [69-75] guaranteeing the development of wearable sensing e-textiles with comprehensive performance.

Apart from the tensile evaluation, performance in piezore-sistive compression was also studied because of its conductive nature, elasticity, and porous hydrogel structure. Generally, the pressure sensing mechanism is based on the deformation of the porous structure in the carbon-gel ink and the increased contact area of the cell wall, resulting in electrical resistance changes. [76] When the external pressure is released, it can spring back to its original state given by the ability of elasticity and recovery resistance, leading to a stable and repeatable response to external pressure stimuli. Accordingly, the enhancement in relative pressure resistance changes of the PA-CPCNT-Fe/PVA sensor was determined by comparing it with PA-Fe/PVA and PA-CNT-Fe/PVA (Figure S19a, Supporting Information). The increase in sensitiv-

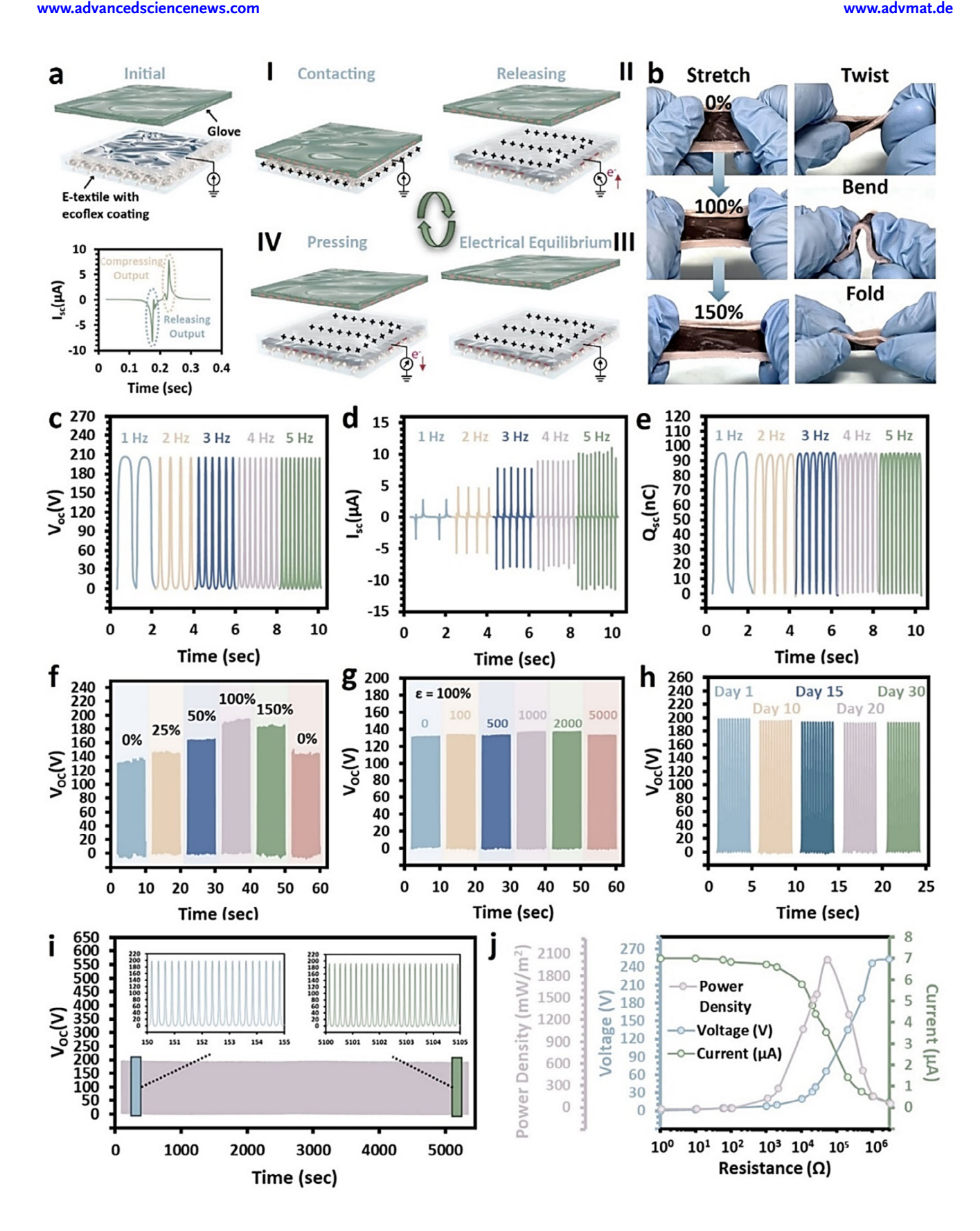
ity was also found by increasing CPCNT content from 0.1 to 0.5 wt.% (Figure S19b, Supporting Information). The compressive force-induced deformation of PA-CNT-Fe/PVA showed a stable cyclic compressing-releasing with different pressures and different frequencies in which a slow increase in resistance changes under higher pressure because the conductive pathway would approach saturation upon continuous pressing (Figure S19c,d, Supporting Information). The durability and stability toward different deformations, as well as wearability, enabled it to detect wider ranges of activities in real-time applications and human-machine interaction.

2.5. Electrical Output Performance of the PA-CPCNT-Fe/PVA Textile-Based TENGs

Triboelectric nanogenerators (TENGs) are promising energy harvesters that effectively capture mechanical energy and transform it into electrical energy. Conductive hydrogels have emerged as a promising electrode material for constructing flexible TENGs. [77-81] The stretchability and flexibility of the PA-CPCNT-Fe/PVA gel made it an ideal choice as an electrode for textilebased TENG. Figure 5a shows the structural design of PA-CPCNT-Fe/PVA TENG in which Ecoflex elastomer was employed as the triboelectric layer, and the PA-CPCNT-Fe/PVA printed textile electrode connected to the external conductive copper wires was encapsulated in the Ecoflex triboelectric layers to create the flexible textile-based TENG. The operating principle was in the single-electrode mode and was based on the coupling effect of contact electrification and electrostatic induction. As schematically illustrated, the Ecoflex coated on the hydrogel surface worked as the negative friction layer and the glove worked as the positive friction layer. At the initial state, the opposite polarities of the glove and the Ecoflex elastomer generated equivalent charges when they were in full contact, under the triboelectric effect (Figure 5a,I). When the glove was separating from the Ecoflex elastomer, the positive charges in the PA-CPCNT-Fe/PVA hydrogel electrode started to balance the unbalanced negative charges at the Ecoflex elastomer interface. Then, electrons flow instantaneously through the copper foil from the ground to the hydrogel electrode layer with electrostatic induction, resulting in an instantaneous electric current (Figure 5a,II). Upon full separation, the induced negative charges in the hydrogel electrode layer completely equilibrated the positive charges on the Ecoflex elastomer, obtaining an electrostatic equilibrium to terminate a flow of free electrons (Figure 5a,III). When the glove layer approached the elastomer again, the aforementioned process was returned and the transient electrons were transported from the hydrogel electrode layer through the external circuit to the ground, generating a reverse current (Figure 5a,IV). By repeating the contactseparation cycle between the glove and the Ecoflex elastomer, the PA-CPCNT-Fe/PVA textile-based TENG generates a continuous alternating current. The fabricated TENGs also showed enough flexibility under stretching, twisting, bending, and folding (Figure 5b).

The potential of the PA-CPCNT-Fe/PVA textile-based TENG as a wearable energy harvester was quantitatively investigated by its electrical output performance. Note that the power generation characteristics of the single-electrode PA-CPCNT-Fe/PVA

1521495, 0, Downloaded from https://aktuatect.onlinelibrary.vitej.com/doi/10.002/ahm.20241570 by HONG KONG POLYTECHNIC UNIVERSITY HU NG HOM, Wiley Online Library on [26/09/2025]. See the Terms and Conditions on Wiley Online Library vitej.com/eter-and-conditions) on Wiley Online Library for rules of use; OA articles are governed by the papilicable Centwice Commons Licensed







textile-based TENG were tested with an effective area of 3×3 cm². Figure 5c-e addressed the variation of the open circuit voltage $(V_{\rm OC})$, the short circuit current $(I_{\rm SC})$, and the short circuit transferred charge (Q_{SC}) at different test frequencies. A stable performance of V_{OC} and Q_{SC} was kept at a peak value of 200 V and 95 nC, respectively; whilst I_{SC} was increased from $\approx 2.5 \,\mu\text{A}$ to 10 μA when the frequency increased from 1 to 5 Hz. It suggests that the motion speed could affect the current output performance which was consistent with previously reported studies.^[82] The voltage performance was also increased by increasing the loading (Figure S20, Supporting Information). Being a flexible and wearable device, the stability of the signal output voltage upon deformation is important. The electrical output performance of the PA-CPCNT-Fe/PVA printed textile-based TENG (1 \times 3 cm²) was studied with different strain levels (Figure 5f). An increase in $V_{\rm OC}$ was found from 130 V to 190 V when the PA-CPCNT-Fe/PVA textile-based TENG was elongated from 0% to 100%; whilst it started to decrease to 180 V on the contrary as the strain level further increased to 150%. The output performance was returned to the initial voltage when the stretch was released. The variation from rising to decline contributed to the change in the contact area between the two triboelectric layers caused by strain deformation, consistent with the Poisson effect during the tensile test. [83,84] Importantly, it could keep in responsible range even after multiple times operating stretching cycles, indicating promising fatigue resistance (Figure 5g). In addition, durability and storage time were crucial in maintaining good performance and providing a good guarantee for practical applications. It performed good long-term stability that barely changes of output voltages were found after being stored at 40 RH% and 25 °C for different times over 30 days, due to the water retention property of the glycerol in hydrogel and the coating Ecoflex (Figure 5h). Besides, the electrical output performance remained stable after ≈20 000 times contact-dissociation cycles

The energy output capability of the PA-CPCNT-Fe/PVA textile-based TENG was then evaluated by connecting to an external circuit with a variety of resistors in series from 1 k Ω to 3 G Ω . The output voltage and output current were measured, and the instantaneous power density (P) was calculated by: $P = \frac{I^2R}{A}$ where R, I, and A represent the resistance, the output current, and the contact area, respectively. As shown in Figure 5j, following Ohm's law, the output voltage of the PA-CPCNT-Fe/PVA textile-based TENG increased with the increase of the external resistance, while the current showed the opposite trend. The maximum output power density is calculated as 2036.9 mW m $^{-2}$ when the external load resistance is \approx 50 M Ω , as shown in Figure 5j. The average power density was also calculated as 627.59 mW m $^{-2}$ (Figure S21, Supporting Information).

2.6. Practical Applications of PA-CPCNT-Fe/PVA in Wearable Energy Harvesting and Sensing Devices

Based on the electrical output performance of the as-made TENG, a self-charging system (Figure 6a) composed of a PA-CPCNT-Fe/PVA textile-based TENG, a rectifier bridge, a capacitor, and electronics was developed to evaluate the energy harvesting capability in external circuits for its potential application as a power source to drive wearable electronics. First, the charging property was measured by using commercial capacitors with different capacitances (1.5, 4.7, 10, and 22 µF), and the results are shown in Figure 6b. The time taken to charge the capacitors with a capacitance of 1, 4.7, and 10 µF to 1.5 V was 7.2, 23, and 50 s, respectively. After charging for 120 s, the capacitors with the capacitance of 22 µF reached a voltage of 1.6 V. In addition, the charging speed increased significantly with increasing operating frequency from 1 to 5 Hz (Figure 6c). This is because the higher the contact-detachment frequency between the friction-charged layer, the more friction charge will be generated. These results suggested that the charging ability of the PA-CPCNT-Fe/PVA textile-based TENG was affected by the capacitance of the capacitor and the operating frequency. To better confirm the self-powering ability in real-time applications, the PA-CPCNT-Fe/PVA textile-based TENG was employed to drive commercial electronics with repeatable charging cycles under a tapping frequency of 3 Hz without any additional power supply unit. Figure 6d shows that 100 s is taken to power an electrical calculator followed by 20 s of discharging time with a 10 μF capacitor; whilst 50 s is taken to power an electrical stopwatch followed by 10 s of discharging time with a 4.7 μF capacitor (Figure 6e), respectively. A hand-tapping demonstration of charging a commercial stopwatch was also presented (Video S3, Supporting Information), ensuring the capability of a power source for self-powered wearable electronics. Furthermore, different pattered LEDs could be easily lit up by hand tapping the PA-CPCNT-Fe/PVA TENG with a pair of gloves (Figure 6f; Video S4, Supporting Information), demonstrating it as a wearable energy harvester. Moreover, the voltage output performance and flexibility of the PA-CPCNT-Fe/PVA TENG also make it a self-powered sensor for human motion detection. For example, it could differentiate the bending angles of finger joints with related output signals, followed by the detection of wrist and elbow bending and foot stepping (Figure 6g). With the contact-separation working mode, it is worth enough to sense and translate the pointing messages of Morse code such as "TENG", "SOS" and "POLYU", compressed by finger movements (Figure 6h). The above applications have successfully ensured that the PA-CPCNT-Fe/PVA textilebased TENG can be used as both a wearable self-powered device to harvest energy and to monitor human physiological activities,

Figure 5. Working mechanism and electrical output performance of the PA-CPCNT-Fe/PVA E-textile TENG. a) Schematic diagram and working mechanism of the PA-CPCNT-Fe/PVA E-textile TENG. b) Photos of the PA-CPCNT-Fe/PVA E-textile TENG showing its flexibility. c) I_{SC} , d) V_{OC} , and e) Q_{SC} of the PA-CPCNT-Fe/PVA E-textile TENG under different frequencies (1–5 Hz). f) V_{OC} of the PA-CPCNT-Fe/PVA E-textile TENG at various tensile strain levels (0–150%) and recovery states. The initial length is 10 mm, and the contact frequency is 3 Hz. g) V_{OC} of the PA-CPCNT-Fe/PVA E-textile TENG after being stretched for different numbers of cyclic cycles. h) Long-term stability of the PA-CPCNT-Fe/PVA E-textile TENG under continuous impact in 30 days. i) Durability and stability test of the PA-CPCNT-Fe/PVA E-textile TENG under continuous impact for 20000 cycles at a force of 10 N and frequency of 5 Hz. The insets exhibit detailed V_{OC} of the initial and end cycles. j) Dependence of the output voltage, output current, and output power density with the various external load resistances.

1521495, 0, Downloaded from https://advanced.onlinelibrary.viety.com/doi/10.002/adma.20241579.7b y HONG KONG POLYTECHNIC UNIVERSITY HU NG HOM, Wiley Online Library on [26/09/2025]. See the Terms and Conditions on Wiley Online Library for rules of use; OA articles are governed by the papilicable Centwice Commons Licensed Commons Licensed Conditions on the Conditions of the Commons of the Common of the Comm

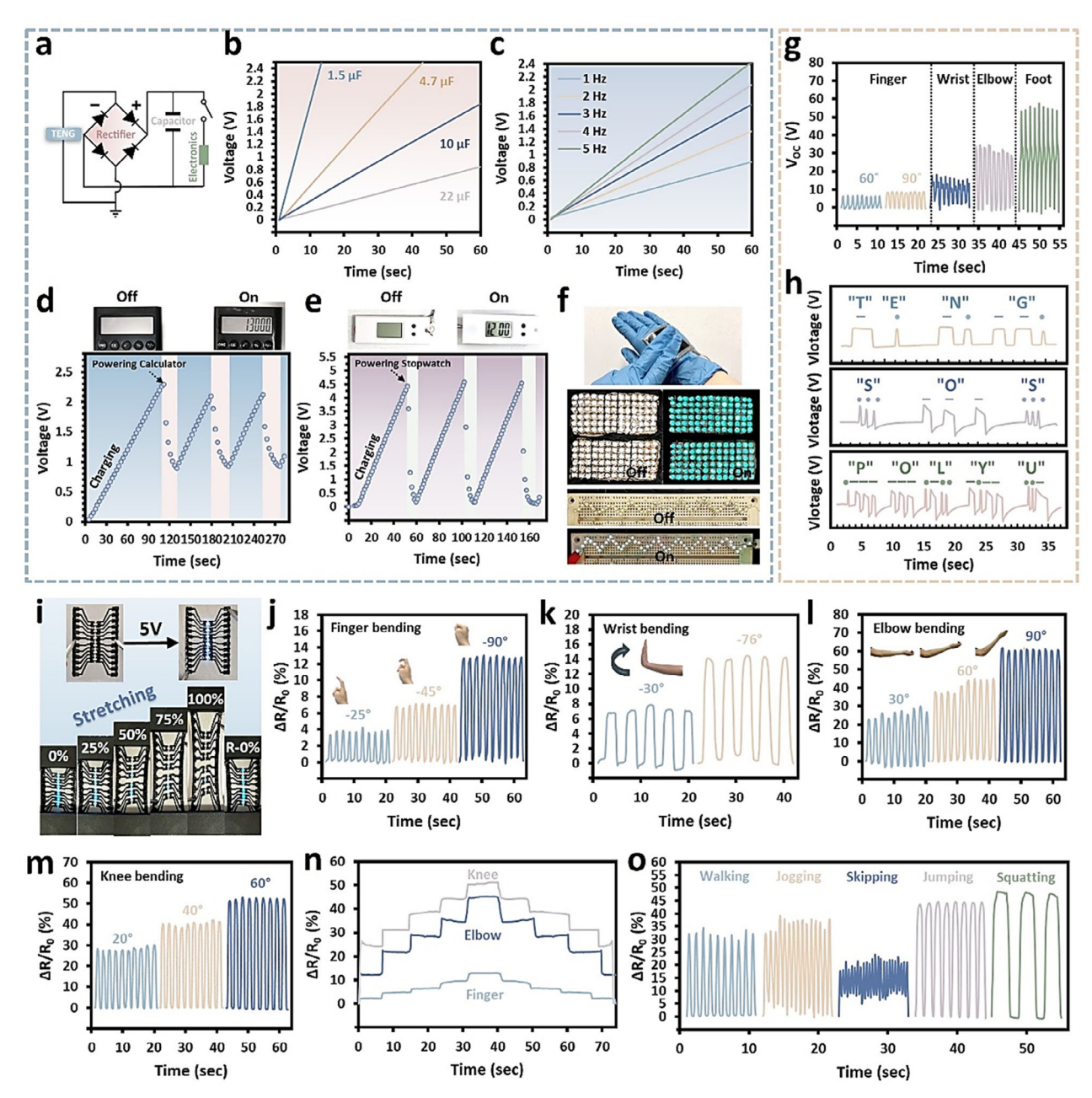


Figure 6. Practical energy harvesting and sensing applications of the PA-CPCNT-Fe/PVA E-textile. a) Working circuit of the self-powered system. Charging ability of the PA-CPCNT-Fe/PVA E-textile TENG b) for different capacitor capacities and c) at different frequencies from 1 to 5 Hz as a power source supply. Demonstration of self-powered electronic devices: d) digital calculator with voltage curves of 22 µF storage capacitors and e) digital stopwatch with voltage curves of 10 µF storage capacitors from hand tapping. f) Photograph of the LED lighting from hand tapping. g) Demonstration of real-time self-powered sensing applications of the PA-CPCNT-Fe/PVA E-textile for finger, wrist, and elbow bending, and foot stepping. h) Reliable sensing signals of the PA-CPCNT-Fe/PVA E-textile TENG in different morse code wordings: TENG, SOS, and POLYU. i) Photographs showing the ability of flexible circuits to power LEDs and resistance change upon different strain levels for real-time motion monitoring. j) finger, k) wrist, l) elbow, and m) knee bending at different angles. n) Real-time step-hold sensing of finger, elbow, and knee. o) Corresponding signals of walking, jogging, skipping, jumping, and squatting.

showing potential for energy supply and signal transmission ap-

Apart from self-powered sensing, the strain-resistance ability of the PA-CPCNT-Fe/PVA also offers promising potential for real-time motion monitoring. Being a flexible circuit, it was able to power several LEDs with an external power supply (Figure 6i). Upon stretching, the decrease in LED lighting further confirmed the resistance change of the PA-CPCNT-Fe/PVA, ensuring that the stable signal responds to strain-based deformation. As shown in Figure 6j-m, the PA-CPCNT-Fe/PVA textile-





based sensors could distinguish the bending angles of finger, wrist, elbow, and knee joints in which the obtained signals responded stably and sensitivity to continuous action changes. Furthermore, a returnable step-hold signal result was collected from full flexion to full extension and returned for each finger (Figure 6n), indicating the accuracy of the sensing signal in small-large scales. Furthermore, the PA-CPCNT-Fe/PVA textile-based sensors could detect the differences in continuous body motions, such as walking, jogging, skipping, jumping, and squatting, by attaching to the leg (Figure 6o) in which the detail successive amplitudes are presented in Figure S22 (Supporting Information). As a result, such sensing potential could further develop in the field of human—machine interaction (HMI).

2.7. Practical Applications of PA-CPCNT-Fe/PVA Printed E-textiles for Human-Machine Interaction

It is feasible to fabricate smart wearable electronics using the PA-CPCNT-Fe/PVA gel ink with good comfort and flexibility. Through DIW printing, integrated fabric-based sensing textiles (e.g., smart glove and sleeve) could be prepared by depositing conductive traces with designed patterns. As schematically illustrated in Figure 7a, the general HMI system is developed with five main steps. First, a smart integrated textile-based unit is obtained by printing a set of sensing units on target locations. The good adhesiveness and flexibility of the gel ink offer it a proper fit on the skin during movement (inset: perfect fitting at joint under curving). Then, the real-time sensing results are collected repeatedly by the multi-channel acquisition and are used to form a database for later signal processing. A series of algorithmic processes are taken to normalize and classify the data via neural networks. Subsequently, the designed program can recognize the signals and take actions after proper machine learning in which a terminal display is also involved to convert signals analog to digital signals presentation in real-time HMI demonstration of both gesture recognition and dexterous manipulation systems. Figure 7b–d concludes the human gesture recognition system for real-time hand gesture recognition. Five different sign languages (e.g., "How are you", "All right", "Having meal", "I love you", and "Thank you") were identified with good repeatability and stability in which various sets of featuring signals could be seen simultaneously corresponding to the PA-CPCNT-Fe/PVA module on each finger (Figure 7b; Figure S23, Supporting Information). Subsequently, the sign languages were successfully recognized with visual messages displayed on the screen in real-time (Figure 7c) The output reliability of the gesture-to-recognition translation system was verified by repeating various hand gestures continuously with 100% accuracy (the normalized confusion matrix shown in Figure 7d). Video S5 (Supporting Information) also displays a real-time demonstration of the gesture-to-recognition translation

Apart from the gesture-to-recognition translation system, the PA-CPCNT-Fe/PVA integrated e-textile showed potential in the development of a robotically assisted gesture-to-manipulation translation system. The procedure included three major parts: 1) The resistance change of gesture components is first collected by

multi-channel acquisition. The collected data is initialized and converted, followed by data normalization. 2) The processed data (database) undergoes grouping, data classification and identification in neural networks, consisting of convolutional layers of CNN, LSTM and attention. 3) After deep learning and training, it can consequently control the robot to complete corresponding hand actions. It was essentially proved by the demonstration of controlling the robotic arm and hand for different target motions and conditions. To achieve a more precise signal transmission, 10 patterned sensing units were incorporated into the functional glove, and each placement of the sensor was referred to the joints of the hand. As shown in Figure 7e, two pairs of hand joints (top), including metacarpophalangeal joints (i.e., no. 1-5) and proximal interphalangeal joints (i.e., no. 6-10), are involved in the control of the robotic hand (bottom). By moving the hand, 10 sensors reflect the resistance changes of each finger joint and respond to specific signal patterns. The real-time sensing results of the seven postures are addressed in Figure 7f. The robotic hand could interact with each motion successfully to give correct and continuous recognition and manipulation (Figure 7g; Video S6, Supporting Information). The effective and good reliability could also be found in the normalized confusion matrix with 100% accuracy in each motion recognition (Figure S24, Supporting Information).

A demonstration of robotic arm manipulation was further presented. As shown in Figure 8a, a glove-sleeve integrated smart textile was printed with four sensing units in which two sensors on the thumb and the index refer to the clap of the robotic, a sensor unit on the wrist controls the small joint motion of the robotic arm and a sensor on the elbow responds to the big joint motion of the robotic arm, respectively. Similarly, the glovesleeve e-textile could realize the movement of the robotic arm to give an accurate response, achieving interaction between humans and machines. For example, when the human elbow moves inward, the big joint of the robotic arm responds with the same posture. A similar result could also be seen in wrist bending and finger movements. 6 sets of designed motion combinations were collected from simple single-joint motions to more complicated and combined motions (Figure 8b). After data classification and deep learning, the gesture-to-manipulation system is developed successfully and can operate in real-time continuously, as shown in Video S7F (Supporting Information). The normalized confusion matrix is also generated, as shown in Figure S25 (Supporting Information), where 100% accuracy is obtained to support the reliable output. With the above robotic hand and arm demonstration, it is believed that more specific situations can be achieved by the interaction between the glove-sleeve etextile and the combined robotic hand-arm. Figure 8c displays the combined system of the robotic hand and arm, corresponding to the integrated smart textile. Generally, the action was done by three major movements: 1) The big joint of the robotic arm moves down to focus on the target subject. 2) The robotic hand moves to grab the ball or cloth by bending all fingers or only the thumb and index, respectively. 3) The robotic hand picks up the object successfully and releases it eventually. Such specific actions involved more complicated movements for handling a ball and a cloth. The real-time sensing results of controlling the robotic hand-arm for grabbing and releasing a ball and soft cloth were recorded, respectively (Figure 8d). It further ensured the SCIENCE NEWS

1521495, 0, Downloaded from https://advanced.onlinelibrary.viety.com/doi/10.002/adma.20241579.7b y HONG KONG POLYTECHNIC UNIVERSITY HU NG HOM, Wiley Online Library on [26/09/2025]. See the Terms and Conditions on Wiley Online Library for rules of use; OA articles are governed by the papilicable Centwice Commons Licensed Commons Licensed Conditions on the Conditions of the Commons of the Common of the Comm

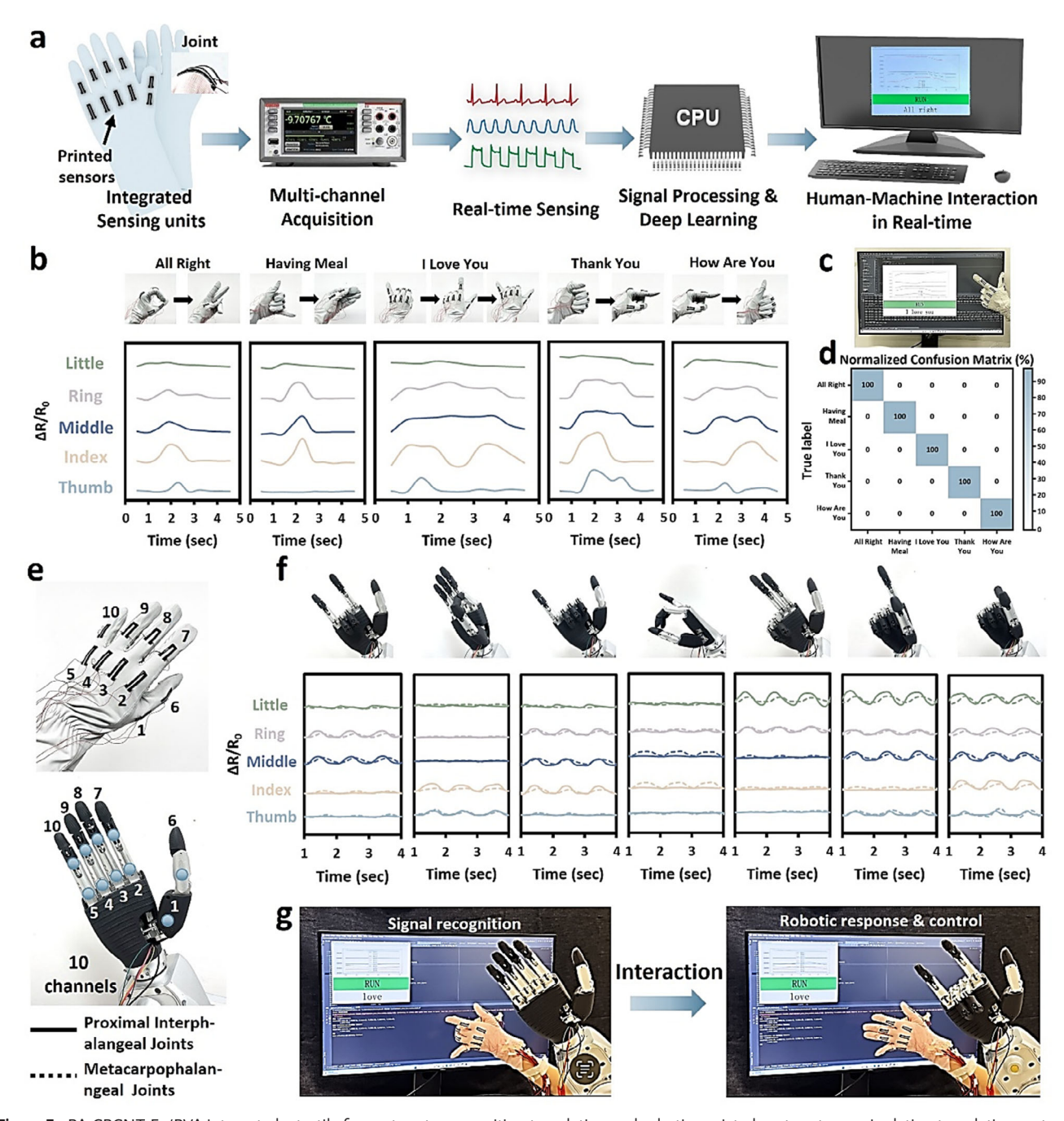


Figure 7. PA-CPCNT-Fe/PVA integrated e-textile for gesture-to-recognition translation and robotic-assisted gesture-to-manipulation translation system. a) Schematic diagram of PA-CPCNT-Fe/PVA integrated e-textile in achieving human—machine interaction (HMI). b) Photograph of electronic gloves composed of PA-CPCNT-Fe/PVA printed sensing units showing five sign languages and real-time electrical signals corresponding to the sign language for each finger. c) The real-time screen display of sign language gestures of "I LOVE YOU". d) The normalized confusion matrix of the gesture-to-recognition translation system. e) Photographs of the smart glove (top) and robotic hand (bottom) with corresponding 10 signal points to the 3D printed e-textile glove. f) Real-time electrical signals of the hand motions. g) The real-time demonstration of gesture-to-recognition and manipulation translation.

feasibility and stability of the PA-CPCNT-Fe/PVA e-textile as a reliable sensor to give data signals and good accuracy of machine learning and response. The real-time demonstration of both "pick-up" exercises is displayed in Figure 8e,f and Video S8 (Supporting Information). As a result, the integrated textile-based

smart modules based on the PA-CPCNT-Fe/PVA exert significant potential in the field of HMI, including sign language translation for the deaf signer, robotic manipulation, virtual reality, patient rehabilitation training for hand injuries, and future artificial intelligence.

1521495, 0, Downloaded from https://advanced.onlinelibrary.viety.com/doi/10.002/adma.20241579.7b y HONG KONG POLYTECHNIC UNIVERSITY HU NG HOM, Wiley Online Library on [26/09/2025]. See the Terms and Conditions on Wiley Online Library for rules of use; OA articles are governed by the papilicable Centwice Commons Licensed Commons Licensed Conditions on the Conditions of the Commons of the Common of the Comm

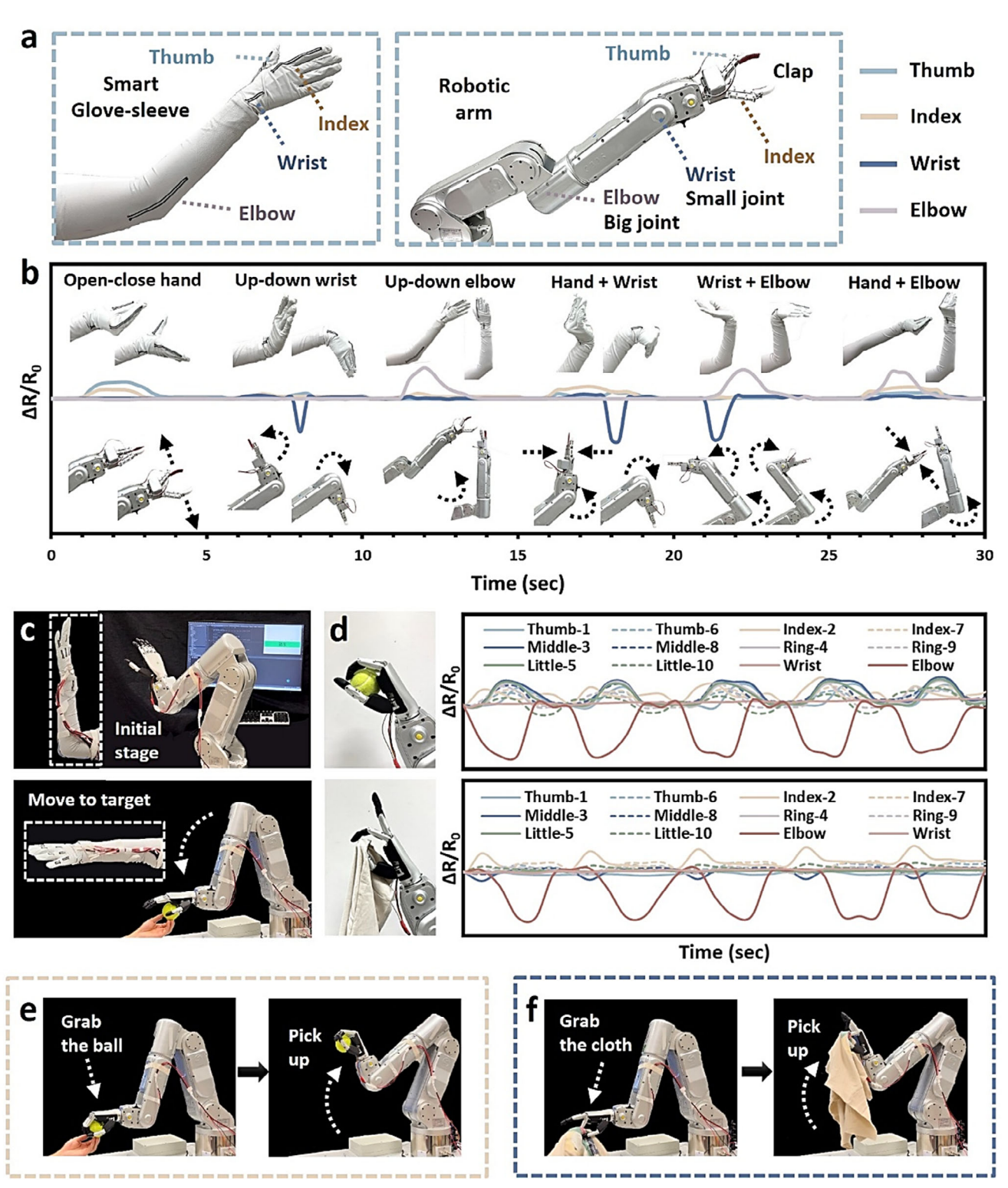


Figure 8. PA-CPCNT-Fe/PVA integrated e-textile for robotic-assisted gesture-to-manipulation translation system (Robotic arm). a) Photograph of smart glove and sleeve composed of PA-CPCNT-Fe/PVA printed sensing units and the corresponding robotic arm system. b) Real-time electrical signals of the hand, wrist, and elbow movement, corresponding to the robotic arm. c) Photo images of the set-up of robotic hand and arm demonstration for the "pick-up" exercise at initial stage (top) and activated stage (down). d) Real-time electrical signals for grabbing a ball and cloth. Practical demonstration of the gesture-to-manipulation system for e) grabbing a ball and f) grabbing a cloth.

ADVANCED MATERIALS

3. Conclusion

In summary, the study presents a cottonseed-derived DIW carbon gel-based ink with a stable and conductive ionic polymer network for the development of soft printing electronic textiles. The incorporation of CP helps generate CNTs with effective dispersibility and biocompatibility which facilitates the stable interactive bonding with the PA-Fe/PVA polymer chain, promoting reliability in conductivity, mechanical properties, stretchability, durability, and reusability. The PA-CPCNT ink enables the direct design of intricate circuits and multifunctional wearable electronics with proper adhesiveness through DIW printing on diverse substrates, including polymers and textiles. Flexible and conductive traces can be facilely prepared and exploited in a wide range of printed electronic textiles, such as flexible circuits, smart sensors, and TENGs. More encouragingly, smart integrated e-textiles can be developed for wearable artificial intelligence and humanmachine interaction, including sign language recognition, and robotic manipulation. Therefore, it envisions that such an attempt to build versatile, biocompatible, and robust bioelectronic platforms can advance the future development of printing wearable electronics and soft electronic textiles.

4. Experimental Section

Materials: Multi-wall carbon nanotubes (MWCNT) were purchased from Shenzhen Suiheng Technology Co., Ltd. (Shenzhen, China) with a purity of >98%, a diameter of <15 nm, and length of 5–15 μm, and a specific surface area of more than 190 m² g $^{-1}$. Cottonseed peptone was obtained from Macklin, Co., Ltd. PA (50 wt.% in water) solution, and glycerol (99%, extra pure) was offered by Acros Organics, Co., Ltd. Anhydrous iron trichloride (FeCl $_3$) was purchased from Shanghai Macklin Biochemical Co., Ltd. PVA (degree of hydrolysis: 99%, Mn: 100 000) was purchased from Chem Co., Ltd.

Preparation of CPCNT Electroconductive Gel-Ink: To prepare CPCNT ink, cottonseed peptone (0.02 g) was dissolved in deionized water (10 mL) to obtain a cottonseed peptone solution. MWCNTs (0.01 g) were dispersed in the cottonseed peptone solution under continuous mechanical stirring. Subsequently, the mixture was sonicated for 15 min under 750 W power using a probe sonicator (VCX750, SONICS & MATERIALS, INC.). Finally, the resultant suspension was centrifuged at 3500 rpm twice to remove undispersed MWCNTs.

Preparation of PA-CPCNT-Fe/PVA Ionic Hydrogel: Owing to the homogeneous dispersion in water, CPCNT gel-ink can be properly compounded with a biodegradable ionic polymer solution to form a biocompatible sensing unit. The CPCNT gel-ink was mixed with glycerol uniformly to prepare a binary solvent. Then, 25 wt.% of phytic acid (PA) and 0.5 wt.% of FeCl $_3$ were added into the above solvent under continuous mechanical stirring to achieve a homogeneous solution. To obtain polymer gel, 10 wt.% of polyvinyl alcohol (PVA) was added to the PA-CPCNT-Fe mixture and dissolved by stirring at 90 °C for 2 h.

Direct Ink Printing of PA-CPCNT-Fe/PVA Hydrogel Inks: The hydrogel direct ink printing was conducted on a direct ink writing (DIW)-based 3D microelectronic printer. To achieve stable and optimal 3D printing, an air pressure of 30 kPa, and a printing speed of 120 mm min $^{-1}$ were chosen for the printing nozzle of $100{-}500\,\mu\text{m}$, where the printed traces were continuous and uniform, and their diameters were nearly the same as that of the nozzle. The direct printed structures were printed at room temperature with a humidity level of 40–60%, and once the printing was completed, the printed structures were further cured by thawing and freezing.

Fabrication of PA-CPCNT-Fe/PVA e-textile TENG: Ecoflex-30 silicone rubber was used in which the base and the curing solution were mixed at a weight ratio of 2:1, and were fully stiffed for 30 min to obtain a complete mixture. The mixture was first poured into a pre-prepared mold to form

the base layer with the same size as the PA-CPCNT-Fe/PVA e-textile and was then dried in the oven to obtain half-curing. The PA-CPCNT-Fe/PVA e-textile was placed on the half-cured Ecoflex film which was still tacky enough to adhere to other surfaces. Then, the Ecoflex mixtures were uniformly integrated into the PA-CPCNT-Fe/PVA e-textile by a blade-coating method for obtaining the top triboelectric layer. Subsequently, the coating was fully cured at room temperature and further dried in the oven at 60 °C. Due to the superior adhesion capabilities of Ecoflex, it bonds firmly to the textile substrates

Development of Gesture-To-Recognition and Robotic-Assisted Gesture-To-Manipulation Translation System: The sensing units were printed on commercial gloves and sleeves via DIW printing (DB100 module, Prtronic). Each sensing unit was connected to a channel of the multi-channel acquisition (DAQ6510) for collecting the state of the hand and arm. The robotic hand (TisRobot) and robotic arm (S6H4D-Plus, Nanjing Seed Intelligent Technology Co., Ltd) were used for the gesture-to-manipulation translation system. The acquired electrical signals were analyzed by a program designed with Python and underwent data classification and identification in neural networks. With deep learning, the designed program could recognize the sign language and control the robotic system successfully. When a specific gesture was executed, this group of electrical signals matched the electrical signal corresponding to the pattern of the gesture, and then the program displayed the relevant information and manipulated the robotic system to implement the recognition and translation of the gesture.

Characterization and Measurement: Morphology, microstructure, and elemental analysis of CPCNT ink and PA-CPCNT-Fe/PVA gel were assessed through Transmission Electron Microscope (JEOL JEM-2010), Scanning Electron Microscope ("Hitachi" Model TM-3000 Tabletop), Raman Spectrometer (Bayspec Nomadic III Laser Raman Confocal Microscope), Fourier Transform Infrared Spectrometer (FTIR) (Perkinelmer" FT-IR Spectrum 100 + Autoimage IR Microscope), XPS spectrometer (ES-CALAB 250XIb from Thermo Fisher Scientific, UV-vis spectrophotometer (Lambda 750, PerkinElmer, Inc.) and Rigaku Ultima model IV X-ray diffractometer (XRD). To investigate the mechanical properties and electrical resistance of the PA-CPCNT-Fe/PVA gel, real-time resistance was recorded using a Keithley-2400 connecting with a digital multimeter. Concerning electric output measurement of the SaLM-SeCNT E-textile, a Keyboard Life Tester (ZXA03) was utilized to operate the periodic contactseparation action with different forces and frequencies. The open-circuit voltage (V_{OC}) , short-circuit current (I_{SC}) and short-circuit charge transfer (Q_{SC}) were measured by an electrometer (Keithley 6514 system). The force signal was monitored by DAQ (Dewetron, Dewe-2600 DAQ system). Testing the wearables was carried out with the assistance of one human participant volunteer (one author of this article), and informed written consent was obtained from the participant.

Supporting Information

Supporting Information is available from the Wiley Online Library or from the author.

Acknowledgements

The work reported in this paper was funded by The Hong Kong Polytechnic University (Project No. 1-CD43, 1-W34U, 1-WZ1Y). K.Y. Chung would like to thank The Hong Kong Polytechnic University for providing her with a postgraduate scholarship.

Conflict of Interest

The authors declare no conflict of interest.

Data Availability Statement

The data that support the findings of this study are available from the corresponding author upon reasonable request.

www.advmat.de

Keywords

biopolymer, carbon gel, DIW printing, e-textiles, wearable electronics

Received: October 15, 2024 Revised: May 28, 2025 Published online:

- [1] S. Xu, A. Jayaraman, J. A. Rogers, Nature 2019, 571, 319.
- [2] L. Lu, C. Jiang, G. Hu, J. Liu, B. Yang, Adv. Mater. 2021, 33, 2100218.
- [3] M. Liu, Y. Zhang, Y. Zhang, Z. Zhou, N. Qin, T. H. Tao, Adv. Sci. 2022, 9, 2102596.
- [4] D. Rus, M. T. Tolley, Nature 2015, 521, 467.
- [5] S. Chen, S. Jiang, D. Qiao, J. Wang, Q. Zhou, C. Wu, X. Li, R. E. Neisiany, L. Sun, Y. Liu, Small Methods 2023, 7, 2201604.
- [6] S. Jiang, J. Deng, Y. Jin, B. Qian, W. Lv, Q. Zhou, E. Mei, R. E. Neisiany, Y. Liu, Z. You, J. Pan, Bioactive Materials 2023, 21, 313.
- [7] J. Song, S. Chen, L. Sun, Y. Guo, L. Zhang, S. Wang, H. Xuan, Q. Guan, Z. You, Adv. Mater. 2020, 32, 1906994.
- [8] L. Sun, H. Huang, Q. Ding, Y. Guo, W. Sun, Z. Wu, M. Qin, Q. Guan, Z. You, Adv. Fiber Mater. 2022, 4, 98.
- [9] H. Tan, L. Sun, H. Huang, L. Zhang, R. E. Neisiany, X. Ma, Z. You, Adv. Mater. 2024, 36, 2310020.
- [10] D. Gao, J. Lv, P. S. Lee, Adv. Mater. 2022, 34, 2105020.
- [11] M. L. Presti, G. Rizzo, G. M. Farinola, F. G. Omenetto, Adv. Sci. 2021, 8. 2004786.
- [12] Y. Y. Huang, E. M. Terentjev, Polymers 2012, 4, 275.
- [13] L. Chen, S. Y. H. Abdalkarim, H. Yu, X. Chen, D. Tang, Y. Li, K. C. Tam, Nano Res. 2022, 15, 7432.
- [14] C. E. Owens, R. J. Headrick, S. M. Williams, A. J. Fike, M. Pasquali, G. H. McKinley, A. J. Hart, Adv. Funct. Mater. 2021, 31, 2100245.
- [15] T. Li, C. Chen, A. H. Brozena, J. Zhu, L. Xu, C. Driemeier, J. Dai, O. J. Rojas, A. Isogai, L. Wågberg, *Nature* 2021, 590, 47.
- [16] Z. Ouyang, S. Li, J. Liu, H.-Y. Yu, L. Peng, S. Zheng, D. Xu, K. C. Tam, Nano Energy 2022, 104, 107963.
- [17] K. Kurppa, H. Jiang, G. R. Szilvay, A. G. Nasibulin, E. I. Kauppinen, M. B. Linder, Angew. Chem., Int. Ed. 2007, 46, 6446.
- [18] S. Marchesan, M. Prato, Chem. Commun. 2015, 51, 4347.
- [19] Y.-W. Ding, X.-W. Zhang, C.-H. Mi, X.-Y. Qi, J. Zhou, D.-X. Wei, Smart Materials in Medicine 2023, 4, 59.
- [20] M. Liu, S. Jiang, N. Witman, H. Wang, W. Wang, W. Fu, Z. You, *Matter* 2023, 6, 983.
- [21] K. Y. Chung, B. Xu, D. Tan, Q. Yang, Z. Li, H. Fu, Nano-Micro Lett. 2024, 16, 149.
- [22] S. R. Shin, M. R. Farzad, A. Tamayol, M. V. Manoharan, P. Mostafalu, Y. S. Zhang, M. Akbari, S. M. Jung, D. Kim, M. M. Commotto, Adv. Mater. 2016, 28, 3280.
- [23] M. Kumar, M. Tomar, S. Punia, S. Grasso, F. Arrutia, J. Choudhary, S. Singh, P. Verma, A. Mahapatra, S. Patil, *Trends Food Sci. Technol.* 2021, 111, 100.
- [24] M. Kim, S.-C. Jee, S. K. Shinde, B. M. Mistry, R. G. Saratale, G. D. Saratale, G. S. Ghodake, D.-Y. Kim, J.-S. Sung, A. A. Kadam, *Polymers* 2019, 11, 271.
- [25] T. Wedegaertner, K. Rathore, Procedia Environmental Sciences 2015, 29, 124.
- [26] R. R. Balandrán-Quintana, A. M. Mendoza-Wilson, G. R.-C. Montfort, J. Á. Huerta-Ocampo, in *Proteins: Sustainable Source, Processing and Applications*, Elsevier, Amsterdam, Netherlands 2019.
- [27] S. Liang, Z.-D. Wang, Z.-F. Guo, X.-Y. Chen, S.-Q. Li, B.-D. Wang, G.-L. Lu, H. Sun, Z.-N. Liu, H.-Y. Zang, New J. Chem. 2021, 45, 3947.

- [28] C.-F. He, W.-B. Liu, L. Zhang, W.-L. Chen, Z.-S. Liu, X.-F. Li, Aquaculture Nutrition 2023, 2023, 8347921.
- [29] L. Li, X. Xu, B. Wang, P. Song, Q. Cao, Y. Yang, Z. Xu, H. Wang, Composites Communications 2021, 28, 100970.
- [30] Z. Liu, Z. Liu, B. Shu, C. Lian, J. Wu, Q. Wen, J. Wu, Z. Yang, W. Zhou, Y. Hu, J. Appl. Polym. Sci. 2023, 140, 54243.
- [31] Y. Guo, J. Bae, Z. Fang, P. Li, F. Zhao, G. Yu, Chem. Rev. 2020, 120, 7642.
- [32] Z. Tashi, M. Zare, N. Parvin, Mater. Lett. 2020, 264, 127275.
- [33] J. Zhao, Y. Lu, Y. Liu, L. Liu, J. Yin, B. Sun, G. Wang, Y. Zhang, Nano-materials 2023, 13, 380.
- [34] S. Zhang, Y. Zhang, B. Li, P. Zhang, L. Kan, G. Wang, H. Wei, X. Zhang, N. Ma, ACS Appl. Mater. Interfaces 2019, 11, 32441.
- [35] J. Li, Y. Li, Y. Song, S. Niu, N. Li, Ultrason. Sonochem. 2017, 39, 853.
- [36] R. Narayanaswamy, L. K. Wai, N. M. Esa, *Pharmacognosy magazine* **2017**, *13*, S512.
- [37] H. Cheng, Z. He, C. Ford, W. Wyckoff, Q. Wu, Sustainable Chemistry 2020, 1, 256.
- [38] F. B. Kadumudi, M. Hasany, M. K. Pierchala, M. Jahanshahi, N. Taebnia, M. Mehrali, C. F. Mitu, M. A. Shahbazi, T. G. Zsurzsan, A. Knott, Adv. Mater. 2021, 33, 2100047.
- [39] Z. Wang, X. Zheng, T. Ouchi, T. B. Kouznetsova, H. K. Beech, S. Av-Ron, T. Matsuda, B. H. Bowser, S. Wang, J. A. Johnson, *Science* 2021, 374, 193.
- [40] D. Tan, B. Xu, K. Y. Chung, Y. Yang, Q. Wang, Y. Gao, J. Huang, Adv. Funct. Mater. 2024, 34, 2311457.
- [41] D. Tan, B. Xu, Adv. Funct. Mater. 2023, 33, 2306793.
- [42] J. Lu, B. Xu, J. Huang, X. Liu, H. Fu, Adv. Funct. Mater. 2024, 32, 2406901.
- [43] X. Guo, Y. Miao, P. Ye, Y. Wen, H. Yang, Mater. Res. Express 2014, 1, 025403.
- [44] X. Li, L. Yuan, R. Liu, H. He, J. Hao, Y. Lu, Y. Wang, G. Liang, G. Yuan, Z. Guo, Adv. Energy Mater. 2021, 11, 2003010.
- [45] Y. Lin, H. Zhang, H. Liao, Y. Zhao, K. Li, Chem. Eng. J. 2019, 367, 139.
- [46] H. Jiang, Y. Zhu, X. Ye, Z. Yue, L. Wang, J. Xia, J. Xie, C. Jia, ACS Sustainable Chem. Eng. 2020, 8, 9896.
- [47] H. Qi, H. Zhang, X. Wu, Y. Tang, M. Qian, K. Wang, H. Qi, Chem.-An Asian J. 2020, 15, 1281.
- [48] I. Hussain, S. M. Sayed, G. Fu, Int. J. Biol. Macromol. 2018, 118, 1463.
- [49] S. Yang, X. Tao, W. Chen, J. Mao, H. Luo, S. Lin, L. Zhang, J. Hao, Adv. Mater. 2022, 34, 2200693.
- [50] F. Xiao, Z. Chen, H. Wu, Y. Wang, E. Cao, X. Lu, Y. Wu, Z. Ren, Nanoscale 2019, 11, 23027.
- [51] M. Lin, Z. Zheng, L. Yang, M. Luo, L. Fu, B. Lin, C. Xu, Adv. Mater. 2022, 34, 2107309.
- [52] Y. Liu, X. Yu, Y. Guo, Y. Ren, X. Liu, Composites, Part A 2023, 173, 107705.
- [53] J. Yang, R. Bai, B. Chen, Z. Suo, Adv. Funct. Mater. 2020, 30, 1901693.
- [54] R. E. Webber, C. Creton, H. R. Brown, J. P. Gong, *Macromolecules* 2007, 40, 2919.
- [55] M. Li, Y. Lin, Y. Zhang, L. Bian, K. Zhang, Chin. J. Chem. 2023, 41, 2697.
- [56] J.-H. Kim, S.-R. Kim, H.-J. Kil, Y.-C. Kim, J.-W. Park, Nano Lett. 2018, 18, 4531.
 [57] J. Yang, D. Tang, J. As, T. Cheel, T. V. Naumann, D. Zhang, Y. Biekerey.
- [57] J. Yang, D. Tang, J. Ao, T. Ghosh, T. V. Neumann, D. Zhang, Y. Piskarev, T. Yu, V. K. Truong, K. Xie, Adv. Funct. Mater. 2020, 30, 2002611.
- [58] X. Yao, S. Zhang, L. Qian, N. Wei, V. Nica, S. Coseri, F. Han, Adv. Funct. Mater. 2022, 32, 2204565.
- [59] H. Yuan, S. Han, S. Wang, P. Yang, S. Li, H.-Y. Mi, C. Liu, C. Shen, Sens. Actuators, B 2023, 379, 133195.
- [60] S. Han, H. Tan, J. Wei, H. Yuan, S. Li, P. Yang, H. Mi, C. Liu, C. Shen, Adv. Sci. 2023, 10, 2301713.
- [61] H. Liu, X. Wang, Y. Cao, Y. Yang, Y. Yang, Y. Gao, Z. Ma, J. Wang, W. Wang, D. Wu, ACS Appl. Mater. Interfaces 2020, 12, 25334.

.com/terms-and-conditions) on Wiley Online Library for rules of use; OA articles are governed by the applicable Creative Commons License

www.advancedsciencenews.com



- [62] G. Chen, J. Huang, J. Gu, S. Peng, X. Xiang, K. Chen, X. Yang, L. Guan, X. Jiang, L. Hou, J. Mater. Chem. A 2020, 8, 6776
- [63] D. Kong, Z. M. El-Bahy, H. Algadi, T. Li, S. M. El-Bahy, M. A. Nassan, J. Li, A. A. Faheim, A. Li, C. Xu, Adv. Compos. Hybrid Mater. 2022, 5, 1976.
- [64] Y. Zhang, T. Li, L. Miao, P. Kaur, S. Men, Q. Wang, X. Gong, Y. Fang, C. Zhai, S. Zhang, J. Mater. Chem. A 2022, 10, 3970.
- [65] G. Chen, O. Hu, J. Lu, J. Gu, K. Chen, J. Huang, L. Hou, X. Jiang, Chem. Eng. J. 2021, 425, 131505.
- [66] J. Liu, X. Chen, B. Sun, H. Guo, Y. Guo, S. Zhang, R. Tao, Q. Yang, J. Tang, J. Mater. Chem. A 2022, 10, 25564.
- [67] X. Wang, N. Li, J. Yin, X. Wang, L. Xu, T. Jiao, Z. Qin, Sci. China Mater. 2023, 66, 272.
- [68] H. Liu, S. Zhang, Z. Li, T. J. Lu, H. Lin, Y. Zhu, S. Ahadian, S. Emaminejad, M. R. Dokmeci, F. Xu, Matter 2021, 4, 2886.
- [69] B. Tian, K. Zheng, R. Yu, X. Chen, P. Guo, Y. Wu, J. Liang, W. Wu, Chem. Eng. J. 2023, 475, 146197.
- [70] B. Yan, S. Liu, Y. Yuan, X. Hou, M. Zhou, Y. Yu, Q. Wang, C. He, P. Wang, Adv. Funct. Mater. 2024, 34, 2401097.
- [71] S. Jang, J. Y. Choi, E. S. Yoo, D. Y. Lim, J. Y. Lee, J. K. Kim, C. Pang, Composites, Part B 2021, 210, 108674.
- [72] X. Bao, J. Meng, Z. Tan, C. Zhang, L. Li, T. Liu, Chem. Eng. J. 2024, 491, 151918.

- [73] B. Tian, Y. Fang, J. Liang, K. Zheng, P. Guo, X. Zhang, Y. Wu, Q. Liu, Z. Huang, C. Cao, Small 2022, 18, 2107298.
- [74] S. Yang, C. Li, X. Chen, Y. Zhao, H. Zhang, N. Wen, Z. Fan, L. Pan, ACS Appl. Mater. Interfaces 2020, 12, 19874.
- [75] M. Zahid, A. Zych, S. Dussoni, G. Spallanzani, R. Donno, M. Maggiali, A. Athanassiou, Composites, Part B 2021, 220, 108969.
- [76] Y. Ma, Y. Yue, H. Zhang, F. Cheng, W. Zhao, J. Rao, S. Luo, J. Wang, X. Jiang, Z. Liu, 3D ACS Nano 2018, 12, 3209.
- [77] P. Lu, X. Liao, X. Guo, C. Cai, Y. Liu, M. Chi, G. Du, Z. Wei, X. Meng, S. Nie, Nano-Micro Lett. 2024, 16, 206.
- [78] L. Hu, P. L. Chee, S. Sugiarto, Y. Yu, C. Shi, R. Yan, Z. Yao, X. Shi, J. Zhi, D. Kai, Adv. Mater. 2023, 35, 2205326.
- [79] J. Han, Z. Li, C. Fang, X. Liu, Y. Yang, Q. Wang, J. Zhang, B. Xu, Nano Energy 2024, 129, 110080.
- [80] T. Chen, Q. Wei, Y. Ma, Y. Tang, L. Ma, S. Deng, B. Xu, Nano Energy 2024, 127, 109752.
- [81] T. Jing, B. Xu, Y. Yang, M. Li, Y. Gao, Nano Energy 2020, 78, 105373.
- [82] Z. Wang, C. Chen, L. Fang, B. Cao, X. Tu, R. Zhang, K. Dong, Y.-C. Lai, P. Wang, Nano Energy 2023, 107, 108151.
- [83] L. Wang, W. Liu, Z. Yan, F. Wang, X. Wang, Adv. Funct. Mater. 2021, 31, 2007221.
- [84] T. Lei, Y. Wang, Q. Zhang, H. Wang, X. Duan, J. Yan, Z. Xia, R. Wang, W. Shou, X. Li, *Nano Energy* **2024**, *126*, 109633.